UCSF
UC San Francisco Previously Published Works

Title

A transcription factor complex in Dictyostelium enables adaptive changes in macropinocytosis during the growth-to-development transition

Permalink

https://escholarship.org/uc/item/1hm141q2

Authors

Hao, Yazhou
Yang, Yihong
Tu, Hui
et al.

Publication Date

2024-02-01

DOI

10.1016/j.devcel.2024.01.012

Peer reviewed

eScholarship.org Powered by the California Digital Library
University of California

Article

Developmental Cell

A transcription factor complex in *Dictyostelium* enables adaptive changes in macropinocytosis during the growth-to-development transition

Graphical abstract

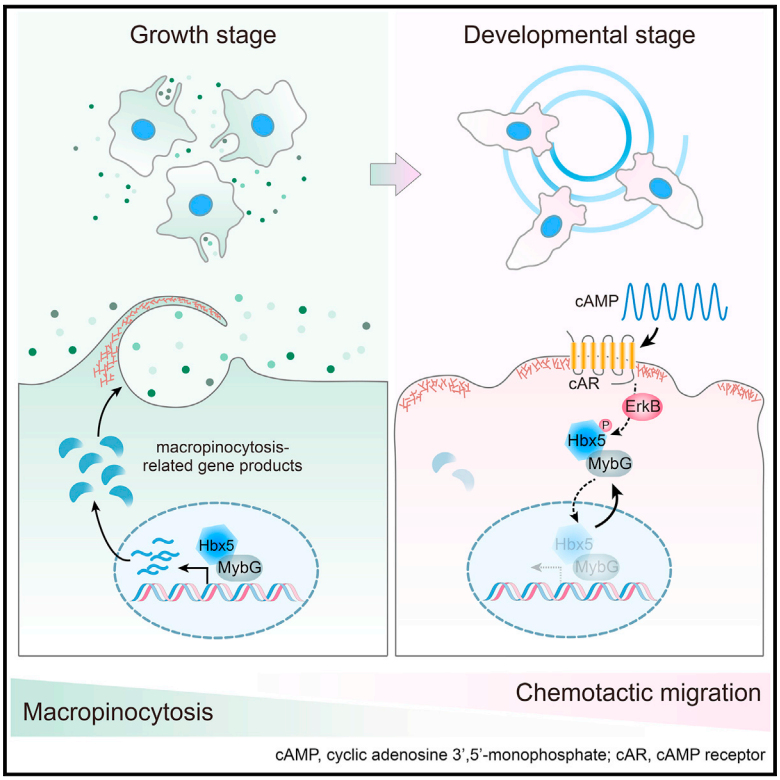

Highlights

- Hbx5-MybG complex maintains macropinocytic activity during growth
- Hbx5-MybG complex responds to cAMP waves during starvation-induced development
- Nuclear exclusion of Hbx5-MybG complex mediates macropinocytosis downregulation
- Hbx5 and MybG enable cell behavior adaptation to changing nutrient conditions

Authors

Yazhou Hao, Yihong Yang, Hui Tu, ..., Bo Li, Lei Li, Huaqing Cai

Correspondence

lei.li@pku.edu.cn (L.L.),
huaqingcai@ibp.ac.cn (H.C.)

In brief

Hao et al. identify a transcription factor complex in *Dictyostelium* cells that promotes macropinocytosis in growing cells and mediates its downregulation during starvation-induced multicellular development. The complex's dynamic nucleocytoplasmic shuttling, regulated by the cAMP oscillation system, orchestrates a population-level adjustment of macropinocytic activity to adapt to changing nutrient conditions.

Hao et al., 2024, Developmental Cell *59*, 1–16
March 11, 2024 © 2024 Elsevier Inc.
https://doi.org/10.1016/j.devcel.2024.01.012

CellPress

Please cite this article in press as: Hao et al., A transcription factor complex in *Dictyostelium* enables adaptive changes in macropinocytosis during the growth-to-development transition, Developmental Cell (2024), https://doi.org/10.1016/j.devcel.2024.01.012

Developmental Cell

CellPress

Article

A transcription factor complex in *Dictyostelium* enables adaptive changes in macropinocytosis during the growth-to-development transition

Yazhou Hao,[1,2,7] Yihong Yang,[1,7] Hui Tu,[3,7] Zhonglong Guo,[4,5,7] Pengcheng Chen,[6] Xiaoting Chao,[1,2] Ye Yuan,[1,2] Zhimeng Wang,[1,2] Xilin Miao,[1,2] Songlin Zou,[1,2] Dong Li,[1] Yanzhi Yang,[4] Congying Wu,[3] Bo Li,[6] Lei Li,[4,*] and Huaqing Cai[1,2,8,*]

[1]Key Laboratory of Biomacromolecules (CAS), National Laboratory of Biomacromolecules, CAS Center for Excellence in Biomacromolecules, Institute of Biophysics, Chinese Academy of Sciences, Beijing 100101, China
[2]College of Life Sciences, University of Chinese Academy of Sciences, Beijing 100049, China
[3]Institute of Systems Biomedicine, Beijing Key Laboratory of Tumor Systems Biology, School of Basic Medical Sciences, Peking University Health Science Center, Peking University, Beijing 100191, China
[4]State Key Laboratory of Protein and Plant Gene Research, School of Advanced Agricultural Sciences, Peking University, Beijing 100871, China
[5]Co-Innovation Center for Sustainable Forestry in Southern China, College of Biology and the Environment, Nanjing Forestry University, Nanjing 210037, China
[6]Department of Engineering Mechanics, Applied Mechanics Laboratory, Institute of Biomechanics and Medical Engineering, Tsinghua University, Beijing 100084, China
[7]These authors contributed equally
[8]Lead contact
*Correspondence: lei.li@pku.edu.cn (L.L.), huaqingcai@ibp.ac.cn (H.C.)
https://doi.org/10.1016/j.devcel.2024.01.012

SUMMARY

Macropinocytosis, an evolutionarily conserved endocytic pathway, mediates nonselective bulk uptake of extracellular fluid. It is the primary route for axenic *Dictyostelium* cells to obtain nutrients and has also emerged as a nutrient-scavenging pathway for mammalian cells. How cells adjust macropinocytic activity in various physiological or developmental contexts remains to be elucidated. We discovered that, in *Dictyostelium* cells, the transcription factors Hbx5 and MybG form a functional complex in the nucleus to maintain macropinocytic activity during the growth stage. In contrast, during starvation-induced multicellular development, the transcription factor complex undergoes nucleocytoplasmic shuttling in response to oscillatory cyclic adenosine 3′,5′-monophosphate (cAMP) signals, which leads to increased cytoplasmic retention of the complex and progressive downregulation of macropinocytosis. Therefore, by coupling macropinocytosis-related gene expression to the cAMP oscillation system, which facilitates long-range cell-cell communication, the dynamic translocation of the Hbx5-MybG complex orchestrates a population-level adjustment of macropinocytic activity to adapt to changing environmental conditions.

INTRODUCTION

Macropinocytosis is an evolutionarily conserved endocytic pathway characterized by the nonselective internalization of large volumes of extracellular fluid. This process involves local remodeling of the actin cytoskeleton to form membrane protrusions, or ruffles, which subsequently close to generate micrometer-sized vesicles known as macropinosomes.[1–3] Newly formed macropinosomes traffic through the endolysosomal system, where their contents are digested and extracted.[4,5]

Macropinocytosis is observed in a variety of cell types and serves diverse functions.[6,7] In the social amoeba *Dictyostelium discoideum*, macropinocytosis facilitates the uptake of nutrients, including amino acids (aa) and glucose, from the growth medium.[8] In mammals, it plays an important role in nutrient acquisition, immune surveillance, synaptic activity regulation, and cell migration.[9–11] Macropinocytosis is hijacked by pathogens, such as viruses and bacteria, to invade cells[12] and is exploited by cancer cells to promote their growth and proliferation in the nutrient-poor tumor microenvironment by scavenging extracellular proteins and fatty acids.[13–18]

Macropinocytic activity is regulated by diverse environmental factors. For example, extracellular calcium is required for constitutive macropinocytosis in macrophages and dendritic cells.[19]

Please cite this article in press as: Hao et al., A transcription factor complex in *Dictyostelium* enables adaptive changes in macropinocytosis during the growth-to-development transition, Developmental Cell (2024), https://doi.org/10.1016/j.devcel.2024.01.012

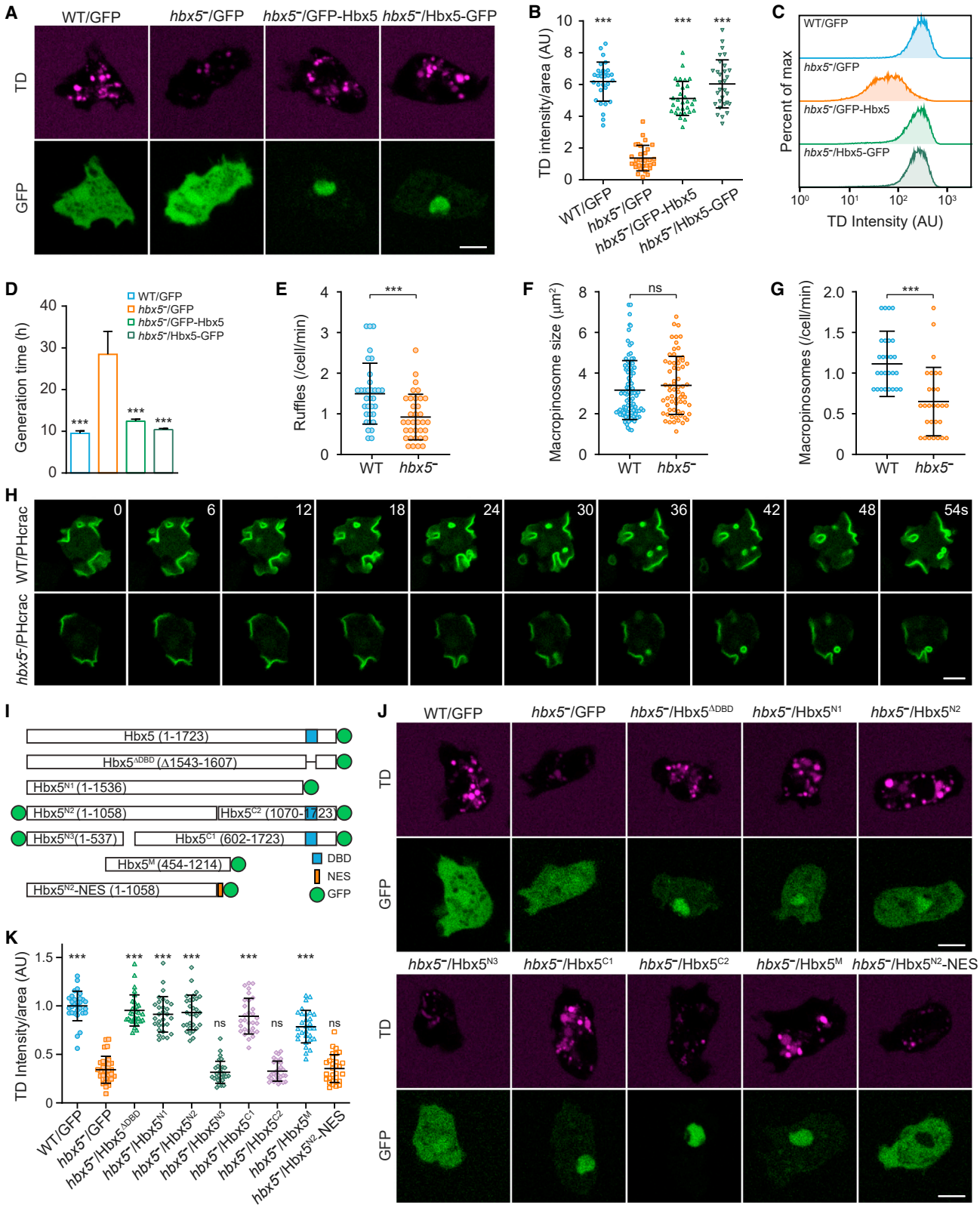

Figure 1. Hbx5 regulates macropinocytosis in vegetative cells

(A and B) Confocal images (A) and quantification (B) of TD uptake in WT cells expressing GFP and *hbx5*⁻ cells expressing GFP, GFP-Hbx5, or Hbx5-GFP (n = 30 for all cell lines).

(legend continued on next page)

Please cite this article in press as: Hao et al., A transcription factor complex in *Dictyostelium* enables adaptive changes in macropinocytosis during the growth-to-development transition, Developmental Cell (2024), https://doi.org/10.1016/j.devcel.2024.01.012

Growth factors, chemokines, and microbial products stimulate macropinocytosis in distinct cell types.[7,20] The depletion of glutamine has been shown to enhance macropinocytosis in pancreatic tumor cells,[21,22] whereas the presence of certain essential aa inhibits macropinocytosis in macrophages.[23] However, the mechanism whereby cells adjust macropinocytic activity in response to environmental changes under different physiological or developmental contexts remains largely unknown.

The laboratory strains of *Dictyostelium*, which contain genetic mutations that allow axenic growth,[24] provide a valuable model for studying macropinocytosis regulation. In nutrient-rich media, the cells grow as individual amoeba and perform macropinocytosis at a high rate for nutrient acquisition.[8] In contrast, upon starvation, up to 10^5–10^6 cells interact and aggregate to form multicellular structures. The early stage of this developmental program (approximately 8–12 h) is under the guidance of oscillatory signals of cyclic adenosine 3′,5′-monophosphate (cAMP). Through coordinated actions of the enzymes that generate and degrade cAMP and the G protein-coupled cAMP receptors, periodic signals are generated, sensed, and relayed throughout the cell population, resulting in propagating waves of cAMP signals, which drive collective cell migration.[25–27] Intriguingly, macropinocytosis is progressively downregulated during this transition from growth to development.[28–30] Although this adaptive cellular behavior has been known for a long time, the underlying mechanism has not been elucidated.

In this study, we identified two transcription factors (TFs), Hbx5 and MybG, which are responsible for maintaining the macropinocytic activity of cell during the growth stage and downregulating it during multicellular development in response to oscillatory cAMP signals. This mechanism enables a large group of cells to synchronously adjust macropinocytic activity for adaptation to changing environmental conditions.

RESULTS

Hbx5 regulates macropinocytosis in vegetative cells

Using a previously described restriction enzyme-mediated insertion (REMI)-based genetic screen approach,[31] we identified Hbx5, a putative homeobox TF, as a regulator of macropinocytosis. For cells cultured in HL5 growth medium, insertion in the *hbx5* genomic locus impaired the uptake of macropinocytic pathway-specific tracers: 70 kDa tetramethylrhodamine isothiocyanate (TRITC)-dextran (TD) and fluorescein isothiocyanate (FITC)-dextran (FD) (Figure S1A).

To confirm this phenotype, we generated *hbx5* knockout (*hbx5*$^-$) cells (Figures S1B–S1E), which exhibited defects in macropinocytosis similar to the REMI mutant. Substantially fewer and less bright TD-containing vesicles were observed in *hbx5*$^-$ compared with wild-type (WT) cells (Figures 1A and 1B). Quantification by flow cytometry and fluorimetric analyses also revealed a marked reduction in the macropinocytic activity of *hbx5*$^-$ cells (Figures 1C and S1F). Consistent with earlier studies demonstrating a critical role of macropinocytosis for axenic growth,[8,24] the generation time increased from ~10 h for WT to ~28 h for *hbx5*$^-$ cells (Figure 1D). The reduced rate of macropinocytosis and growth in *hbx5*$^-$ cells could be fully rescued by expression of GFP-tagged Hbx5, which localized primarily in the nucleus (Figures 1A–1D and S1F).

Macropinosome formation and maturation depend on coordinated actions of actin regulators, phosphoinositides, and small GTPases.[2–4] Plasma membrane ruffles driven by actin polymerization initially evolve into cup-shaped structures, which are organized around patches of PIP_3 and active Ras.[32] PIP_3 is sequentially dephosphorylated to $PI(3,4)P_2$ and PI(3)P to facilitate cup closure and macropinosome maturation.[33,34] At around the same time, Rab5 is recruited to the macropinosomal membrane, followed by conversion to Rab7.[34] We expressed GFP- or RFP-fused sensors for newly polymerized actin (LimEΔcoil), active Ras (Ras-binding domain [RBD]), PIP_3/$PI(3,4)P_2$ (PHcrac), $PI(3,4)P_2$ (TAPP1), and PI(3)P (2×FYVE), as well as Rab5 and Rab7, in WT and *hbx5*$^-$ cells, and observed their distribution by live-cell imaging. The sensors exhibited similar localization in the two cell lines, suggesting that the overall organization of the macropinocytic pathway was unaffected by *hbx5* deletion (Figures S3A–S3C). However, membrane ruffles were formed with a lower frequency in *hbx5*$^-$ cells, leading to a significant decrease in the rate of macropinosome formation (Figures 1E–1H; Video S1). We confirmed that the decrease in macropinocytic uptake was not due to a malfunction in cargo processing along the macropinocytic pathway (Figures S1G and S1H). Additionally, the deletion of *hbx5* did not noticeably alter phagocytosis (Figures S1I and S1J) or cause general defects in actin polymerization (Figures S1K–S1M). Thus, it appears that Hbx5 plays a specific role in regulating the macropinocytic activity of the cell.

Hbx5 contains a predicted homeobox near the C terminus, which is the characteristic DNA-binding domain (DBD) for

(C) Flow-cytometry analysis of TD uptake.
(D) Cell growth measured by generation time.
(E) Quantification of the number of ruffles formed per cell per minute (n = 33 for WT and 35 for *hbx5*$^-$).
(F) Quantification of macropinosome size (n = 92 for WT and 66 for *hbx5*$^-$).
(G) Quantification of the number of macropinosomes formed per cell per minute (n = 30 for WT and 30 for *hbx5*$^-$).
(H) Time-lapse imaging of PHcrac-GFP in WT and *hbx5*$^-$ cells.
(I) Schematic of full-length Hbx5 (1–1,723 aa) and truncation constructs. DBD, DNA-binding domain; NES, nuclear export signal.
(J and K) Confocal images (J) and quantification (K) of TD uptake in WT cells expressing GFP and *hbx5*$^-$ cells expressing GFP or different Hbx5 constructs (n = 30 for all cell lines).
The scatterplots in (B) and (K) show data points with mean and SD; data were from one representative experiment out of three independent experiments; n represents the number of cells analyzed. The plot in (C) was from one representative experiment out of three independent experiments. The plot in (D) shows data points with mean and SEM; data are from three independent experiments. The scatterplots in (E)–(G) show data points with means and SD; data were from at least three independent experiments; n represents the number of cells (E and G) or events (F) quantified. Significance was determined by one-way ANOVA with Dunnett posttest in (B), (D), and (K) and by two-tailed unpaired t test in (E)–(G).
Scale bars: 5 μm in (A), (H), and (J). AUs, arbitrary units in (B) and (K).

Please cite this article in press as: Hao et al., A transcription factor complex in *Dictyostelium* enables adaptive changes in macropinocytosis during the growth-to-development transition, Developmental Cell (2024), https://doi.org/10.1016/j.devcel.2024.01.012

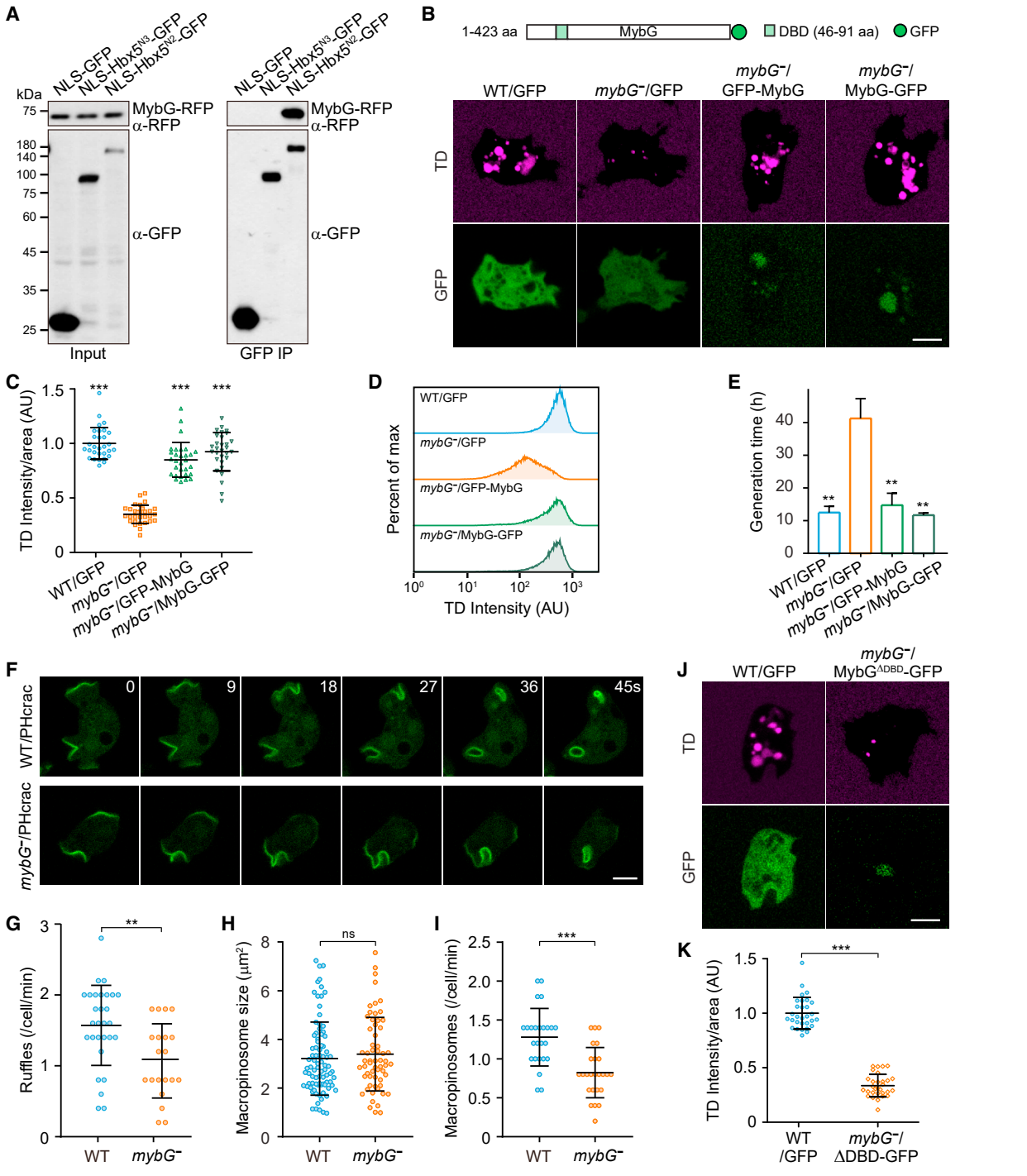

Figure 2. Hbx5 interacts with MybG, which regulates macropinocytosis in vegetative cells

(A) Co-immunoprecipitation (co-IP) of MybG-RFP with NLS-GFP, NLS-Hbx5^{N3}-GFP, or NLS-Hbx5^{N2}-GFP. IP was performed with GFP-trap and samples were probed with GFP or RFP antibody.

(B) Top: schematic of MybG; DBD, DNA-binding domain. Bottom: confocal images of TD uptake in WT cells expressing GFP and *mybG*$^{-}$ cells expressing GFP, MybG-GFP, or GFP-MybG.

(C) Quantification of TD uptake (n = 30 for all cell lines).

(D) Flow-cytometry analysis of TD uptake.

(E) Cell growth measured by generation time.

(F) Time-lapse imaging of PHcrac-GFP in WT and *mybG*$^{-}$ cells.

(G) Quantification of the number of ruffles formed per cell per minute (n = 29 for WT and 20 for *mybG*$^{-}$).

(legend continued on next page)

Please cite this article in press as: Hao et al., A transcription factor complex in *Dictyostelium* enables adaptive changes in macropinocytosis during the growth-to-development transition, Developmental Cell (2024), https://doi.org/10.1016/j.devcel.2024.01.012

homeobox TFs (Figure 1I). To our surprise, the expression of Hbx5 deleted of the homeobox (Hbx5$^{\Delta DBD}$) fully complemented the macropinocytosis defect caused by *hbx5* deletion (Figures 1I–1K). We generated a series of additional truncation constructs (Figure 1I). Hbx5 truncations removing up to 665 aa from the C terminus (Hbx5^{N2}, aa 1–1,058) or 601 aa from the N terminus (Hbx5^{C1}, aa 602–1,723) were still able to rescue the macropinocytosis defect in *hbx5*$^{-}$ cells, but further truncation (Hbx5^{N3}, aa 1–537; Hbx5^{C2}, aa 1,070–1,723) abolished this ability (Figures 1I–1K). Consistently, a fragment covering the middle 761 aa of Hbx5 (Hbx5^{M}, aa 454–1,214) restored macropinocytosis in *hbx5*$^{-}$ cells to near the WT level (Figures 1I and 1K). Therefore, the central region of Hbx5 is required to maintain the efficiency of macropinocytosis in vegetative cells.

Hbx5 associates with MybG to regulate macropinocytosis

Although the classic DBD of Hbx5 is not required, its nuclear localization is still needed for the regulation of macropinocytosis. The addition of an exogenous nuclear export signal (Hbx5^{N2}-NES)—which kept Hbx5^{N2} outside of the nucleus—abolished the ability to rescue *hbx5*$^{-}$ cells (Figures 1I–1K). Thus, we speculated that Hbx5 may associate or cooperate with other regulatory elements in the nucleus for transcriptional regulation of macropinocytosis.

We immunoprecipitated Hbx5^{N2}-GFP—a truncation that restored macropinocytosis in *hbx5*$^{-}$ cells—from cell lysates and performed mass spectrometry analysis for binding partners (Figure S2A). Hbx5^{N3}-GFP—a truncation that failed to rescue *hbx5*$^{-}$ cells—and GFP were included as controls. A nuclear-localization signal (NLS) was fused to all three proteins to increase nuclear accumulation. This experiment revealed that a putative MYB family TF, MybG, was uniquely enriched in the immunocapture of NLS-Hbx5^{N2}-GFP, but not of NLS-Hbx5^{N3}-GFP or NLS-GFP (Figure S2B). Co-immunoprecipitation (co-IP) experiments verified the interaction between MybG and Hbx5^{N2} (Figure 2A).

We generated knockout cells to examine whether MybG is involved in the regulation of macropinocytosis (Figures S2C–S2F). Similar to the deletion of *hbx5*, deletion of *mybG* (*mybG*$^{-}$) strongly impaired the cells' ability to ingest 70 kDa dextran and grow in liquid medium (Figures 2B–2E). These defects were fully rescued by the expression of GFP-tagged MybG, which localized mainly in the nucleus (Figures 2B–2E and S2G). The macropinocytosis defect in *mybG*$^{-}$ cells was also attributed to a reduced rate of ruffle formation (Figures 2F–2I; Video S2), but not aberrant localization of membrane and cytoskeleton regulators (Figure S3) or malfunctions in cargo processing along the macropinocytic pathway (Figures S2H and S2I). Additionally, the deletion of *mybG* did not affect phagocytosis (Figures S2J and S2K) or cause general defects in actin polymerization (Figures S2L–S2N). However, unlike Hbx5, the DBD in MybG is required for its function. Removal of the conserved MYB domain (MybG$^{\Delta DBD}$) did not block the localization of protein in the nucleus but disrupted the ability to rescue *mybG*$^{-}$ (Figures 2J and 2K).

Using different truncations of MybG and Hbx5, we performed additional co-IP experiments and activity assays to examine the functional significance of their interaction. Removal of up to 127 aa from the C terminus of MybG (MybG^{N2}, aa 1–296) minimally affected the ability to rescue the macropinocytosis defect of *mybG*$^{-}$ cells (Figures 3A–3C) or co-immunoprecipitate with Hbx5 (Figure 3D), whereas further truncation (MybG^{N3}, aa 1–207) impaired *mybG*$^{-}$ rescue (Figures 3A–3C) and interaction with Hbx5 (Figure 3D). Removal of the N-terminal 91 aa of MybG (MybG^{C1}, aa 92–423) resulted in a construct that lost the ability to complement *mybG*$^{-}$, likely due to the deletion of the MYB domain, but maintained an interaction with Hbx5 (Figures 3A–3D). Interestingly, MybG^{C1} acted as a dominant negative mutant, inhibiting macropinocytosis when overexpressed in WT cells (Figures 3E and 3F). Thus, it appears that MybG requires not only the DBD, but also the ability to interact with Hbx5, to regulate macropinocytosis. Similarly, for truncations of Hbx5, those that exhibited robust binding to MybG (Hbx5^{N2}, Hbx5^{C1}, and Hbx5^{M}) complemented *hbx5*$^{-}$, whereas those that failed to interact (Hbx5^{N3} and Hbx5^{C2}) were unable to complement (Figures 1I–1K and 3G). These results imply that Hbx5 and MybG function as a protein complex to regulate the macropinocytic activity of vegetative cells.

Hbx5 and MybG co-regulate macropinocytosis-related genes

A comprehensive annotation of macropinocytosis-associated genes is not yet available. To investigate whether Hbx5 and MybG control gene expression related to macropinocytosis, we performed whole transcriptome RNA sequencing (RNA-seq) analysis of WT, *hbx5*$^{-}$, and *mybG*$^{-}$ cells grown in HL5. Compared with WT cells, 1,008 genes were differentially expressed in *hbx5*$^{-}$ cells (Figures 4A and S4A), including 577 upregulated and 431 downregulated genes. Interestingly, 803 (79.7%) of these genes were also differentially expressed in *mybG*$^{-}$ cells (Figure 4A). Consistent with the comparable defects in *hbx5*$^{-}$ and *mybG*$^{-}$ cells (Figures 1A–1H and 2B–2I) and complex formation (Figures 2A, 3D, and 3G), Hbx5 and MybG modulated the vast majority of these genes (768 of 803, 95.6%) in the same direction (Figure S4B).

To pinpoint genes that are directly regulated by the TF complex, we conducted chromatin immunoprecipitation sequencing

(H) Quantification of macropinosome size (n = 93 for WT and 61 for *mybG*$^{-}$).
(I) Quantification of the number of macropinosomes formed per cell per minute (n = 27 for WT and 25 for *mybG*$^{-}$).
(J and K) Confocal images (J) and quantification (K) of TD uptake in *mybG*$^{-}$ cells expressing MybG-GFP or MybG$^{\Delta DBD}$-GFP (n = 30 for both cell lines).
The scatterplots in (C) and (K) show data points with means and SD; data are from one representative experiment out of three independent experiments; n represents the number of cells analyzed. The plot in (D) was from one representative experiment out of three independent experiments. The plot in (E) shows data points with means and SEM; data are from three independent experiments. The scatterplots in (G)–(I) show data points with mean and SD; data are from at least three independent experiments; n represents the number of cells (G and I) or events (H) quantified. Significance was determined by one-way ANOVA with Dunnett posttest in (C) and (E) and by two-tailed unpaired t test in (G)–(I) and (K).
Scale bars: 5 μm in (B), (F), and (J). AUs, arbitrary units in (C) and (K).

Please cite this article in press as: Hao et al., A transcription factor complex in *Dictyostelium* enables adaptive changes in macropinocytosis during the growth-to-development transition, Developmental Cell (2024), https://doi.org/10.1016/j.devcel.2024.01.012

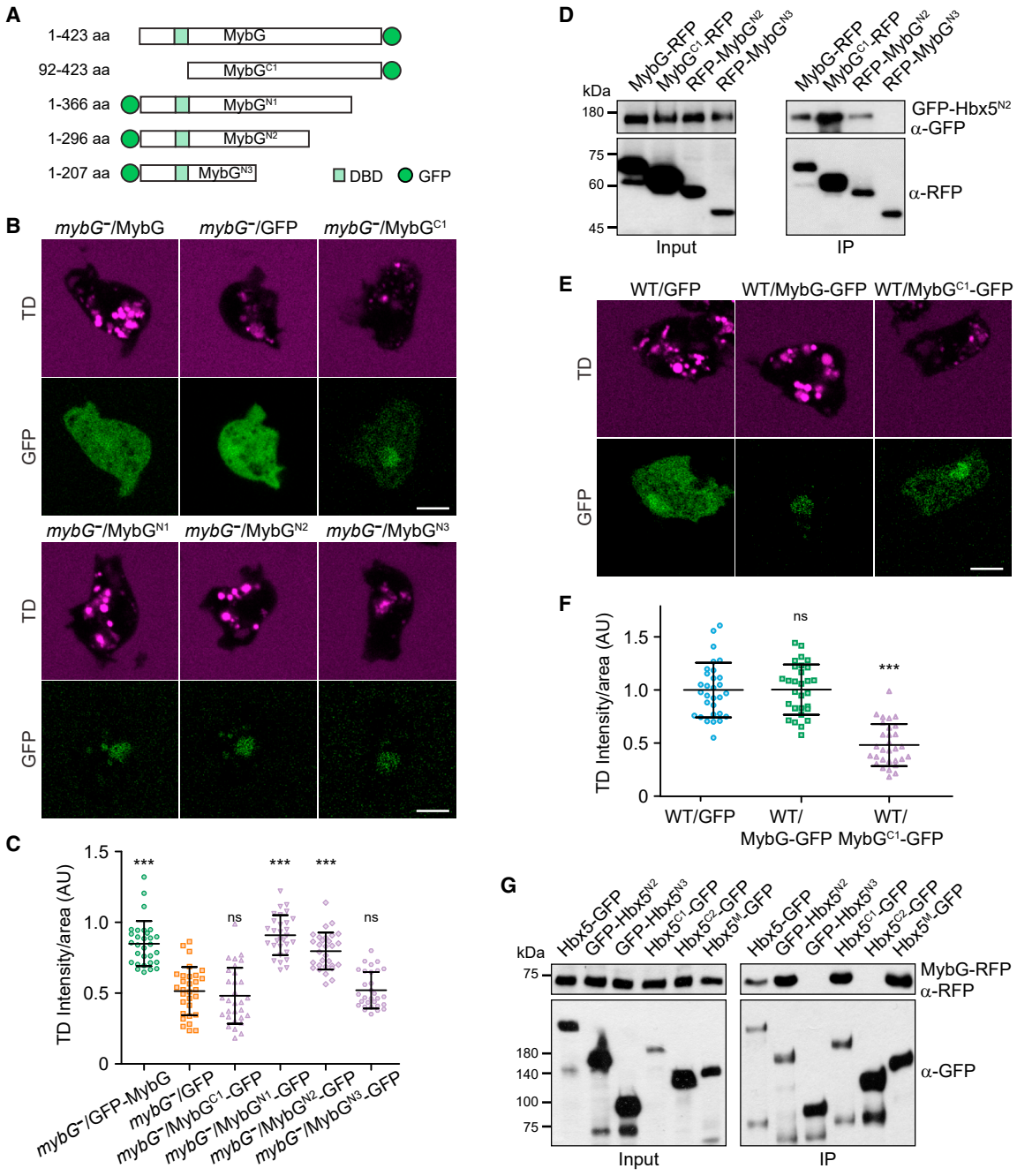

Figure 3. Hbx5 and MybG form a complex to regulate macropinocytosis

(A) Schematic of full-length MybG and truncation constructs.

(B and C) Confocal images (B) and quantification (C) of TD uptake in *mybG*$^-$ cells expressing GFP, MybG-GFP, or GFP-fused MybG truncations (n = 30 for all cell lines).

(D) Co-IP of GFP-Hbx5^{N2} with RFP-fused MybG or MybG truncations. IP was performed with RFP-trap, and samples were probed with GFP or RFP antibody.

(E and F) Confocal images (E) and quantification (F) of TD uptake in WT cells expressing GFP, MybG-GFP, or MybG^{C1}-GFP (n = 30 for all cell lines).

(G) Co-IP of MybG-RFP with GFP-fused Hbx5 or Hbx5 truncations. IP was performed with GFP-trap and samples were probed with GFP or RFP antibody.

The scatterplots in (C) and (F) show data points with mean and SD; data are from one representative experiment out of three independent experiments; n represents the number of cells analyzed. Significance was determined by one-way ANOVA with Dunnett posttest.

Scale bars: 5 μm in (B) and (E). AUs, arbitrary units in (C) and (F).

Please cite this article in press as: Hao et al., A transcription factor complex in *Dictyostelium* enables adaptive changes in macropinocytosis during the growth-to-development transition, Developmental Cell (2024), https://doi.org/10.1016/j.devcel.2024.01.012

CellPress

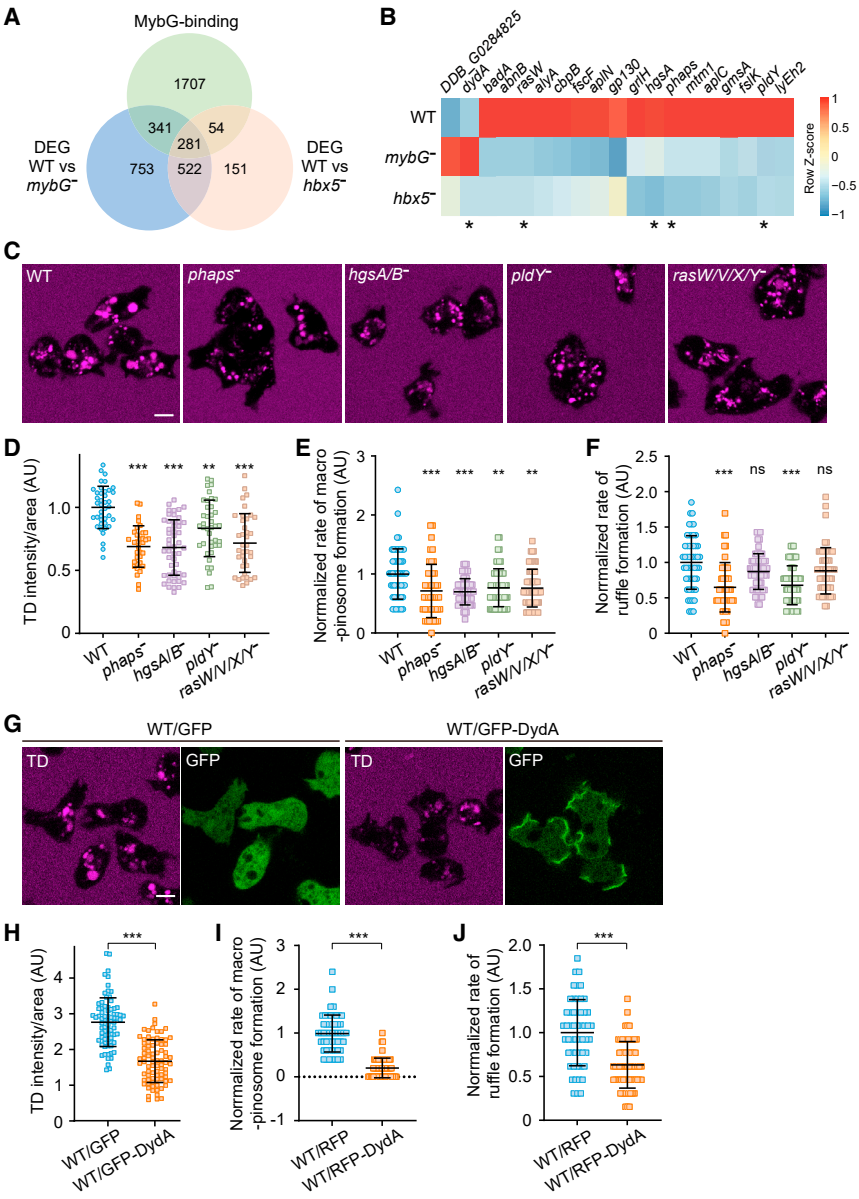

Figure 4. Hbx5 and MybG co-regulate macropinocytosis-related genes

(A) Venn diagram showing the relationships of genes that are directly targeted by MybG and those that are differentially expressed in *hbx5*$^{-}$ and *mybG*$^{-}$. MybG-targeted genes were identified by ChIP-seq analysis of cells expressing MybG-GFP versus those expressing GFP alone. Differentially expressed genes (DEGs) were identified by RNA-seq analysis.

(B) Heatmap showing relative transcript levels of the 19 genes selected for phenotypic analyses. Colors represent *Z* scores generated from the RNA-seq data.

(C and D) Confocal images and quantification of TD uptake in WT, *phaps*$^{-}$, *hgsA*$^{-}$/*B*$^{-}$, *pldY*$^{-}$, and *rasW*$^{-}$/*V*$^{-}$/*X*$^{-}$/*Y*$^{-}$ cells (n ≥ 30 for all cell lines).

(E and F) Quantification of the rate of macropinosome formation (E) and the rate of ruffle formation (F) in the indicated cell lines (n ≥ 40 for all cell lines).

(G and H) Confocal images and quantification of TD uptake in WT cells expressing GFP or GFP-DydA (n ≥ 75 for both cell lines).

(I and J) Quantification of the rate of macropinosome formation (I) and the rate of ruffle formation (J) in WT cells expressing RFP or RFP-DydA (n ≥ 50 for both cell lines).

All scatterplots show data points with mean and SD. Data are from three independent experiments; n represents the number of cells analyzed. Significance was determined by one-way ANOVA with Dunnett posttest in (D)–(F) and by two-tailed unpaired t test in (H)–(J).

Scale bars: 5 μm in (C) and (G). AUs, arbitrary units in (D)–(F) and (H)–(J).

(ChIP-seq) analysis using cells expressing either GFP-tagged MybG or GFP alone. MybG-specific binding peaks were identified in the regulatory regions upstream of the translation start sites of 2,383 genes (Figure 4A). Among the 803 genes commonly affected by deletion of *hbx5* and *mybG*, 281 (35.0%) were found to be directly targeted by MybG and were considered the core set of genes regulated by the complex (Figure 4A; Table S1). We subjected these 281 genes to Gene Ontology (GO) analysis and constructed an association network of enriched GO terms related to cellular components. Interestingly, GO terms associated with macropinocytic, phagocytic, plasma membrane, and cortical cytoskeleton structures, which are macropinocytosis-relevant components, were among the enriched GO terms (Figure S4C).

We selected 19 of the 281 genes for phenotypic analyses. Of these, 17 genes were possibly involved in promoting macropinocytosis, as their expression levels were downregulated in both knockout cells, whereas 2 genes may act as negative regulators of the process because their expression levels were upregulated in the knockout cells (Figure 4B). RT-qPCR analysis was performed to confirm the differential expression profile of these genes (Figures S4D and S4E). Furthermore, Hbx5^{M} and MybG^{N2}, the shortest truncations capable of complex formation and macropinocytosis rescue, were found to completely or partially restore the expression of the majority of these genes when expressed in the respective knockout cell lines (Figures S4D and S4E). The selected genes were either disrupted or overexpressed in WT cells (Table S2), and the effects on macropinocytosis were examined. To overcome redundancy, for genes with closely related homologs or those located in a genomic region containing homologous genes, the disruption also included the homologous genes (Figure S4F; Table S2). We found that cells in which *hgsA/B* (HMG-coenzyme A [CoA] synthase), *phaps* (a putative substrate of protein kinase B), *pldY* (a putative phospholipase), or *rasW/V/X/Y* (Ras family small GTPases) were deleted exhibited significantly reduced macropinocytosis (Figures 4C–4E). Cells overexpressing *dydA* (a putative Ras effector), which localized to macropinocytic cups, also

Please cite this article in press as: Hao et al., A transcription factor complex in *Dictyostelium* enables adaptive changes in macropinocytosis during the growth-to-development transition, Developmental Cell (2024), https://doi.org/10.1016/j.devcel.2024.01.012

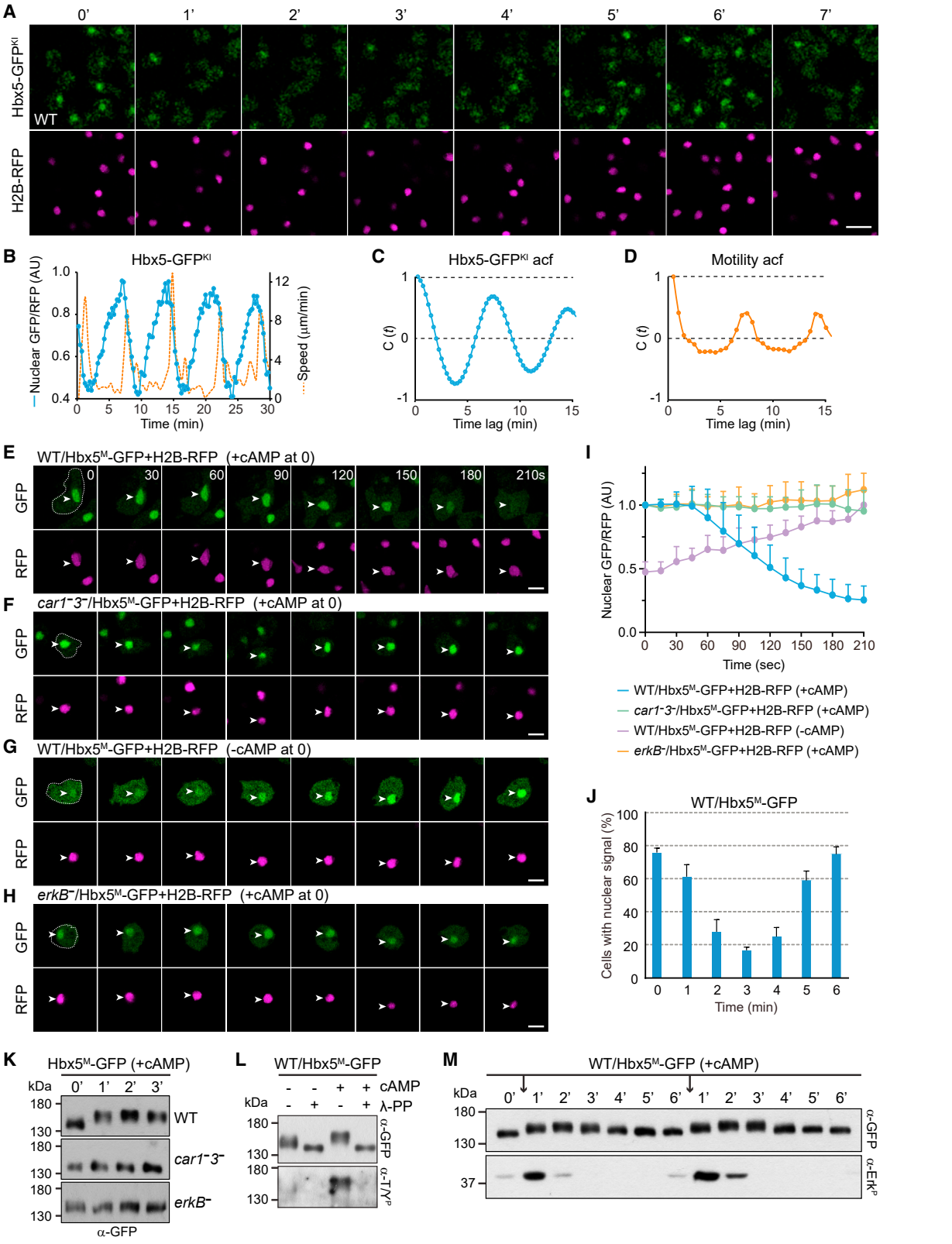

(legend on next page)

Please cite this article in press as: Hao et al., A transcription factor complex in *Dictyostelium* enables adaptive changes in macropinocytosis during the growth-to-development transition, Developmental Cell (2024), https://doi.org/10.1016/j.devcel.2024.01.012

exhibited impaired macropinocytosis (Figures 4G–4I). The deletion of *phaps* or *pldY*, as well as the overexpression of *dydA*, also impacted the frequency of membrane ruffle formation (Figures 4F and 4J). Though further analysis is needed to reveal gene function, these results corroborate the proposed role of Hbx5 and MybG in regulating the expression of macropinocytosis-related genes.

Hbx5 undergoes dynamic changes in localization during early development

Macropinocytosis is downregulated during the transition from growth to multicellular development.[28–30] To investigate the potential role of Hbx5 and MybG in the downregulation of macropinocytosis, in addition to their function in the growth stage, we examined the localization of Hbx5 at different times before and after starvation.

Before starvation, Hbx5-GFP expressed in WT cells localized mainly in the nucleus (Figure S5A; Video S3). This nuclear localization was significantly reduced in cells that chemotactically aggregated to form cell streams, a developmental stage that usually occurs 5–8 h after starvation (Figure S5B; Video S4). RFP-tagged histone H2B was used as a nuclear marker in these experiments. As only nuclear-localized Hbx5 can promote macropinocytosis, this observation suggests that the developmental program may downregulate macropinocytosis over time by reducing the nuclear presence of Hbx5.

Interestingly, during the transition from persistent nuclear localization to cytoplasmic localization, Hbx5 underwent oscillatory nucleocytoplasmic shuttling. This behavior was initially sporadic (Figures S6A and S6B) but became highly synchronized 5–6 h after the onset of development (Figure S6C; Video S5). Hbx5 expressed from the endogenous locus (Hbx5-GFP^{KI}) or the shortest truncation (Hbx5^{M}-GFP) that complemented *hbx5*$^{-}$ cells exhibited similar shuttling behavior (Figures 5A and S6F; Videos S6 and S7).

Several lines of evidence indicate that the shuttling is driven by periodic cAMP signals. First, population-level cAMP oscillation with a period of approximately 6 min is known to occur at this time of development. The period of Hbx5 shuttling was 5.95 ± 0.70 min, similar to that of cAMP oscillation (Figures 5A–5C and S6C–S6H). Second, propagating waves of cAMP have been shown to induce synchronized bursts of cell motility.[35,36] Taking cell speed as a proxy for the cAMP wave phase, Hbx5 likely translocated from the nucleus to the cytoplasm and back to the nucleus in the rising and falling phases of the cAMP wave, respectively (Figures 5B–5D). Consistently, simultaneous imaging of cells expressing Hbx5-GFP or Flamindo2, a cytosolic cAMP indicator,[37] revealed that the decrease in Flamindo2 signal, signifying an increase in cytosolic cAMP levels, was accompanied by the translocation of Hbx5 from the nucleus to the cytoplasm (Figures S7A and S7B). Third, using isolated cells expressing Hbx5^{M}-GFP, we confirmed that Hbx5 moved out of the nucleus when exposed to a uniform stimulation of cAMP in a receptor-dependent manner and re-entered the nucleus when the stimulus was removed (Figures 5E–5G and 5I). Lastly, robust shuttling of Hbx5 could be captured in cell suspensions when pulses of cAMP were applied at 6-min intervals (Figure 5J). In this condition, each addition of cAMP would trigger an amplified response, leading to an increase in cAMP levels lasting for 1–2 min, followed by a return to the basal level before the next pulse.

We previously showed that phosphorylation by the atypical mitogen-activated protein (MAP) kinase ErkB triggers the nuclear-to-cytoplasmic translocation of GtaC, a GATA family TF that exhibits shuttling behavior similar to Hbx5.[36,38] Consistent with possible regulation by phosphorylation, the cAMP-induced translocation of Hbx5^{M}-GFP coincided with a shift in its electrophoretic mobility, which required receptor occupancy (Figure 5K). The slower migrating species could be recognized by a phospho-specific antibody, and the shift was reversed by treatment with λ-protein phosphatase (Figure 5L). In addition, the cAMP-induced translocation and mobility shift were blocked by deletion of *erkB* (Figures 5H, 5I, and 5K). Given that ErkB is necessary for the development of responsiveness to cAMP,[39] we verified its role in Hbx5 translocation using folic acid as the stimuli (Figures S7C–S7E). Furthermore, pulses of cAMP applied at 6-min intervals, which caused periodic activation of ErkB, resulted in periodic changes in the phosphorylation state of Hbx5^{M} (Figure 5M).

The period of cAMP oscillation progressively shortens to approximately 2–4 min as cells form aggregation streams and loose mounds.[35] We found that, when pulses of cAMP were applied to cells at 3-min, rather than 6-min intervals, Hbx5^{M}-GFP failed to repeatedly translocate between the nucleus and cytoplasm and was eventually retained mainly in the cytoplasm (Figures S7F and S7G). Taken together, these results

Figure 5. cAMP oscillation drives nucleocytoplasmic shuttling of Hbx5 during early development

(A) Time-lapse images of WT cells expressing Hbx5 tagged with GFP at the genomic locus (Hbx5-GFP^{KI}) and H2B-RFP during early development.

(B) Plot of changes in the nuclear Hbx5-GFP^{KI}/H2B-RFP fluorescence intensity ratio and averaged cell motility over a 30-min period. Data are from one representative experiment out of at least three independent experiments.

(C and D) Temporal autocorrelation plots.

(E–H) Time-lapse imaging of Hbx5^{M}-GFP translocation in WT (E), *car1*$^{-}$*3*$^{-}$ (F), and *erkB*$^{-}$ (H) upon cAMP stimulation (+cAMP). The cAMP-induced translocation in WT cells was reversed (G) upon the removal of the stimulus (−cAMP).

(I) Quantification of the changes in the nuclear Hbx5^{M}-GFP/H2B-RFP fluorescence intensity ratio over time. Data are from at least three stimulation experiments; mean + SD; n = 10 (n represents the number of cells analyzed).

(J) Cells in suspension were stimulated with pulses of cAMP at 6-min intervals and fixed at the indicated time points in a stimulation cycle. The plot shows the percentage of cells with nuclear signal of Hbx5^{M}-GFP at each time point. Data are from three independent experiments; mean + SEM.

(K) Western blot of samples collected at the indicated time points upon cAMP stimulation. Hbx5^{M}-GFP was expressed in WT, *car1*$^{-}$*3*$^{-}$, or *erkB*$^{-}$ cells. Samples were probed with GFP antibody.

(L) Western blot of samples collected before or after cAMP stimulation in the presence or absence of λ-protein phosphatase (λ-PP). Samples were probed with GFP antibody or phospho-threonine/tyrosine antibody (T/Y^{P}).

(M) Pulses of cAMP applied at 6-min intervals (indicated by the arrows) induced periodic changes in the electrophoretic mobility of Hbx5^{M}-GFP and phosphorylation of ErkB. Samples were probed with GFP antibody or phospho-Erk antibody (Erk^{P}).

Scale bars: 10 μm in (A) and 5 μm in (E)–(H). AUs, arbitrary units in (B) and (I).

Please cite this article in press as: Hao et al., A transcription factor complex in *Dictyostelium* enables adaptive changes in macropinocytosis during the growth-to-development transition, Developmental Cell (2024), https://doi.org/10.1016/j.devcel.2024.01.012

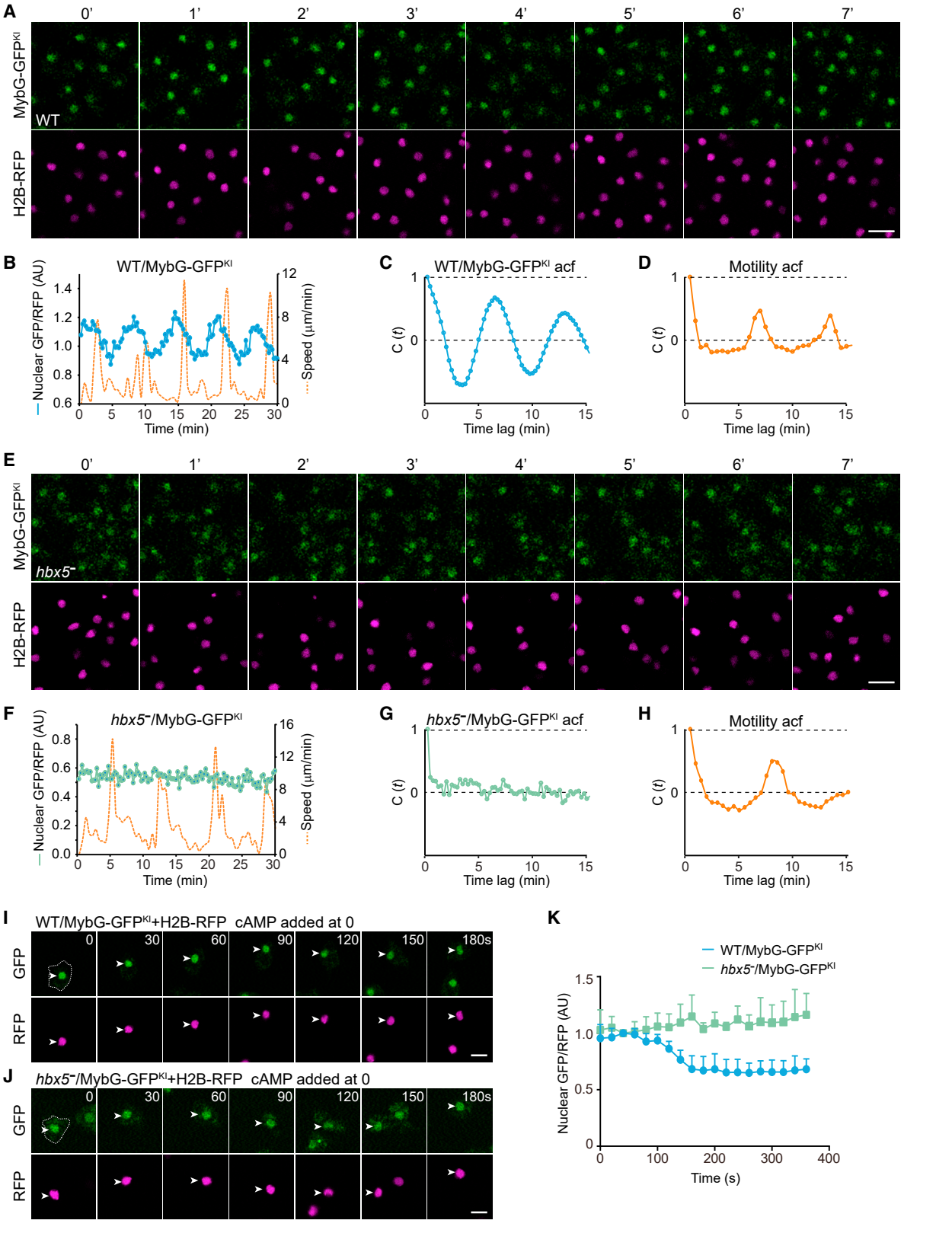

(legend on next page)

Please cite this article in press as: Hao et al., A transcription factor complex in *Dictyostelium* enables adaptive changes in macropinocytosis during the growth-to-development transition, Developmental Cell (2024), https://doi.org/10.1016/j.devcel.2024.01.012

demonstrate that the localization of Hbx5 is actively and dynamically regulated during development. The periodic cAMP signals not only drive the initial synchronized shuttling of Hbx5 but also likely induce its cytoplasmic retention in the later stages of aggregation.

MybG undergoes changes in localization in an Hbx5-dependent manner

Next, we examined the localization of MybG. In vegetative cells and cells that had entered the streaming stage of development (Figures S8A and S8B), a significant fraction of MybG-GFP was found in the nucleus. Thus, at first glance, the localization of MybG appeared to exhibit minimal changes during growth or development. However, imaging MybG-GFP^{KI} cells that developed for 4–5 h and quantifying the nuclear accumulation of MybG revealed an oscillatory pattern similar to that of Hbx5 (Figures 6A and 6B; Video S8). Although in every cycle only an estimated 30% of MybG-GFP^{KI} underwent nuclear-to-cytoplasmic translocation, this correlated each time with an increase in average cell motility, implying that the translocation occurred during the rising phase of the cAMP wave (Figures 6B–6D). The period of MybG shuttling was 6.04 ± 0.57 min, similar to that of Hbx5 shuttling and cAMP oscillation. By directly applying cAMP stimulation, we confirmed the translocation behavior of MybG (Figures 6I and 6K).

Notably, the shuttling of MybG strictly depended on Hbx5. In *hbx5*$^{-}$ cells, the nuclear accumulation of MybG-GFP^{KI} exhibited no apparent periodicity, even in a cell population that was clearly experiencing cAMP waves by displaying rhythmic changes in cell motility (Figures 6E–6H; Video S9). Furthermore, the addition of uniform stimulation of cAMP failed to induce the nuclear-to-cytoplasmic translocation of MybG-GFP^{KI} in *hbx5*$^{-}$ cells (Figures 6J and 6K). These results indicate that at least a fraction of MybG experiences dynamic localization changes during development by forming a complex with Hbx5. Consistently, we found that the expression of Hbx5^{N2}-NES-GFP greatly reduced the nuclear localization of MybG-RFP, but not of MybG^{N3}-RFP, which lacked the ability to interact with Hbx5 (Figures S8C–S8E). Likewise, the expression of MybG-NES-RFP, which exhibited reduced nuclear accumulation, decreased the nuclear localization of Hbx5-GFP (Figures S8F and S8G).

cAMP oscillation and TF shuttling modulate the downregulation of macropinocytosis during development

The observed localization changes in Hbx5 and MybG during development indicate a possible link between macropinocytosis downregulation and cAMP-induced TF shuttling. We hypothesized that, with the occurrence and progressive acceleration of cAMP oscillations, the TF complex will be expelled repeatedly from the nucleus and retained in the cytoplasm for prolonged periods of time, leading to a progressive downregulation of macropinocytic activity. We conducted the following experiments to further test the hypothesis.

First, we examined the effect of disrupting Hbx5 shuttling on macropinocytosis downregulation. To this end, we fused tandem NLSs (2×NLS) to Hbx5 (Figure 7A). Although the inserted sequence did not block the cAMP-induced nuclear-to-cytoplasmic translocation of Hbx5, it impeded the process, causing Hbx5 to remain in the nucleus for an extended period (Figures 7B and 7C). We compared the change in macropinocytic activity in cells expressing either Hbx5-GFP or 2×NLS-Hbx5-GFP following starvation. Macropinocytic activity in cells expressing Hbx5-GFP was decreased after 6 h and almost abolished after 10 h of development (Figures 7D–7F). However, the process was delayed in cells expressing 2×NLS-Hbx5-GFP (Figures 7D–7F), indicating that compromised Hbx5 shuttling interferes with the downregulation of macropinocytosis.

Next, we investigated how variation in the frequency of cAMP oscillation affects the downregulation of macropinocytosis. To remove the interference of spontaneously generated cAMP, we utilized *crac*$^{-}$ cells, which do not produce cAMP but can respond to externally applied cAMP pulses.[40] The shuttling of Hbx5 in *crac*$^{-}$ cells appeared to be synchronized with cAMP oscillation, which normally occurs during early development, similar to shuttling in WT cells. Specifically, cAMP pulses of 6-min intervals induced repeated translocation of Hbx5, which effectively excluded it from the nucleus for a significant period of time in each stimulation cycle (Figures 7G and S9). With lower-frequency pulses (12- and 24-min intervals), Hbx5 responded by exiting the nucleus for an equivalent amount of time but returned and remained in the nucleus for the rest of the stimulation cycle (Figures 7G and S9A). Thus, higher-frequency cAMP oscillations were expected to shorten the duration of Hbx5 in the nucleus (Figure 7H), which would then expedite the process of macropinocytosis downregulation. In line with the prediction, cells with the same developmental age that were stimulated with cAMP pulses of 6-min intervals exhibited an accelerated downregulation of macropinocytosis compared with those stimulated with less frequent pulses (Figures 7I–7K). Higher-frequency cAMP pulses were also found to cause a greater reduction in the expression of several macropinocytosis-promoting genes regulated by the Hbx5-MybG complex (Figure 7L). On the other hand,

Figure 6. MybG undergoes nucleocytoplasmic shuttling in an Hbx5-dependent manner

(A) Time-lapse images of WT cells expressing MybG tagged with GFP at the genomic locus (MybG-GFP^{KI}) and H2B-RFP during early development.

(B) Plot of the changes in the nuclear MybG-GFP^{KI}/H2B-RFP fluorescence intensity ratio in WT cells and averaged cell motility over a 30-min period. Data are from one representative experiment out of at least three independent experiments.

(C and D) Temporal autocorrelation plots.

(E) Time-lapse images of *hbx5*$^{-}$ cells expressing MybG-GFP^{KI} and H2B-RFP during early development.

(F) Plot of the changes in the nuclear MybG-GFP^{KI}/H2B-RFP fluorescence intensity ratio in *hbx5*$^{-}$ cells and averaged cell motility over a 30-min period. Data are from one representative experiment out of at least three independent experiments.

(G and H) Temporal autocorrelation plots.

(I and J) Time-lapse images show changes in the localization of MybG-GFP^{KI} in WT (I) or *hbx5*$^{-}$ (J) cells upon a uniform stimulation of cAMP.

(K) Quantification of the changes in the nuclear MybG-GFP^{KI}/H2B-RFP fluorescence intensity ratio over time. Data are from at least three stimulation experiments; mean + SD; n = 10 for both cell lines (n represents the number of cells analyzed).

Scale bars: 10 μm in (A) and (E) and 5 μm in (I) and (J). AUs, arbitrary units in (B), (F), and (K).

Please cite this article in press as: Hao et al., A transcription factor complex in *Dictyostelium* enables adaptive changes in macropinocytosis during the growth-to-development transition, Developmental Cell (2024), https://doi.org/10.1016/j.devcel.2024.01.012

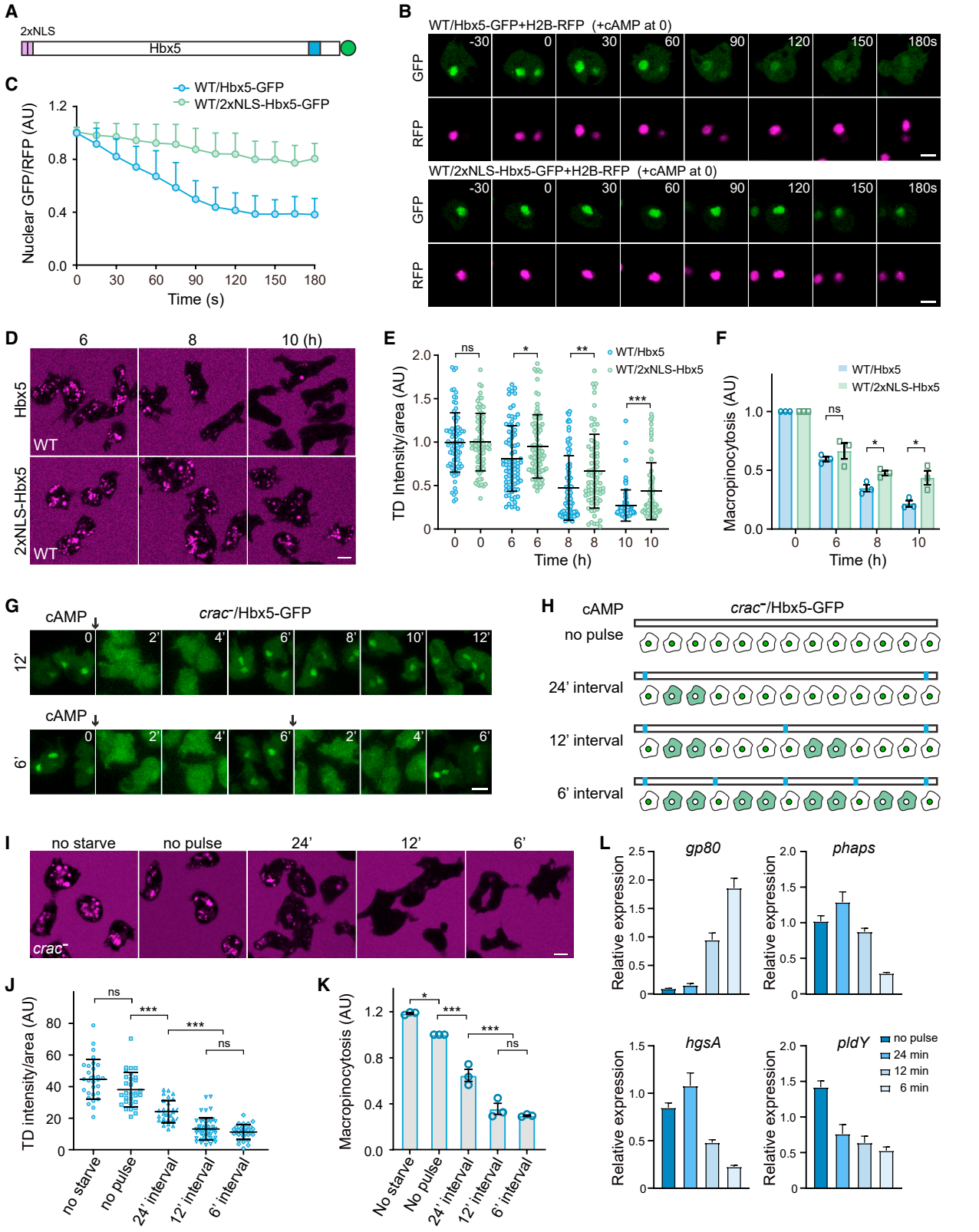

Figure 7. Hbx5 shuttling is linked to macropinocytosis downregulation during development

(A) Schematic of 2×NLS-Hbx5-GFP. NLS, nuclear localization signal.

(B) Time-lapse imaging of the translocation of Hbx5-GFP and 2×NLS-Hbx5-GFP upon cAMP stimulation.

(legend continued on next page)

Please cite this article in press as: Hao et al., A transcription factor complex in *Dictyostelium* enables adaptive changes in macropinocytosis during the growth-to-development transition, Developmental Cell (2024), https://doi.org/10.1016/j.devcel.2024.01.012

gp80, which is recognized as the target of GtaC, another shuttling TF,[36] exhibited an opposite pattern (Figure 7L). Collectively, these experiments suggest that the developmental regulation of macropinocytosis is achieved by modulating the nuclear localization of the Hbx5-MybG TF complex via self-organized cAMP oscillations.

DISCUSSION

Macropinocytosis in *Dictyostelium* cells is known to be influenced by nutrient abundance and developmental state. The cells exhibit a high rate of macropinocytosis during growth but downregulate it during starvation-induced multicellular development. Although this adaptive cellular behavior was first recognized 40 years ago,[30] the underlying mechanism remains elusive. The data presented in this study support a working model in which cAMP oscillation-dependent relocalization of a pair of TFs drives the adaptive change in macropinocytic activity (Figure S10). Hbx5 and MybG form a functional complex in the nucleus to regulate a cohort of genes for maintaining the macropinocytic activity of vegetative cells. During starvation-induced development, the emerging cAMP oscillations repeatedly expel Hbx5 and the associated MybG from the nucleus, leading to a progressive downregulation of macropinocytosis. As cAMP oscillations accelerate during the later stages of aggregation, the TF complex is mainly confined to the cytoplasm, effectively switching off macropinocytosis (Figure S10).

The cAMP relay system that produces rhythmic cAMP signals is not only a fascinating example of biological oscillation, but also acts as a mediator of long-range cell-cell communication. Research has shown that cAMP signals that are periodically generated and propagated regulate the collective migration of a large population of cells by serving as chemoattractant gradients and differentiation signals.[25–27] In this study, we demonstrated that oscillatory cAMP signals also contribute to the repression of macropinocytic activity. Due to the cAMP-driven translocation of the Hbx5-MybG complex, the degree of macropinocytosis downregulation positively correlates with the number of cAMP pulses the cells encounter during development, rather than their developmental age. Thus, by linking the expression of macropinocytosis-associated genes to the cAMP relay system, the regulation of macropinocytic activity can be synchronized in a large cell population over an expanded territory.

As macropinocytic cups and pseudopods compete for signaling and cytoskeletal machinery,[32,41] downregulating macropinocytosis during development could facilitate the acquisition of chemotactic ability, which is crucial for the successful formation of cell-aggregation structures. Interestingly, we showed previously that the gain of chemotactic activity is under the transcriptional regulation of another shuttling TF. GtaC, a GATA family TF, decodes oscillatory cAMP signals and induces collective migration through dynamic nucleocytoplasmic shuttling.[36,42] Furthermore, we found that the shuttling of both GtaC and Hbx5 is directed by repeated cycles of phosphorylation and dephosphorylation, mediated in part by the ErkB kinase, a core component of the cAMP relay system.[26,36,38] Sharing similar regulatory mechanisms may allow the two transcriptional programs to coordinate activities, potentially leading to an integrated change in cell behavior and function. It is yet to be determined whether ErkB directly phosphorylates Hbx5 and the precise location where this reaction occurs (Figure S10).

Analyzing how macropinocytosis is regulated during the growth-to-development transition by Hbx5 and MybG provides further insights into the signaling that governs macropinocytosis. First, *Dictyostelium* and mammalian cells seem to employ opposing strategies when coping with nutrient stress. Similar to starvation-induced downregulation of macropinocytosis, the depletion of specific aa, such as arginine and lysine, results in reduced macropinocytosis in *Dictyostelium*.[31] In contrast, depletion of aa, specifically glutamine, enhances macropinocytosis in pancreatic tumor cells.[21,22] These differences may reflect divergent survival strategies that have evolved in different cell types. In *Dictyostelium*, nutrient scarcity could trigger multicellular development, a process that benefits from reduced macropinocytosis. Conversely, mammalian cells, which lack this alternative route, may instead resort to increased macropinocytosis for nutrient scavenging. Second, although the change in the localization of the Hbx5-MybG complex plays a critical role in the development-induced downregulation of macropinocytosis, it does not seem to contribute to other conditions that lead to reduced macropinocytosis. We have found that depleting arginine and lysine from the growth medium, adding bacteria as a nutrient source, or applying an agarose overlay, conditions known to suppress macropinocytosis,[28,29,41] did not alter the nuclear localization of Hbx5 (Figures S9B–S9E). These observations suggest that the regulation of macropinocytosis involves other prominent sensory and signaling pathways.

(C) Quantification of the changes in the nuclear GFP/RFP fluorescence intensity ratios over time. Data are from at least three stimulation experiments; mean + SD; n = 10 (n represents the number of cells analyzed).
(D–F) Confocal images (D) and quantification (E and F) of TD uptake in the indicated cell lines at 6, 8, and 10 h of development. The plot in (E) shows data points with means and SD from one representative experiment; $n \geq 70$ for all conditions (n represents the number of cells analyzed). The plot in (F) shows normalized macropinocytic activity; means and SD; n = 3 (n represents the number of experiments analyzed).
(G) *crac*$^-$ cells expressing Hbx5-GFP were developed in suspension with cAMP pulses applied at 6- or 12-min intervals. Cells were taken at the indicated time points before (time 0) or after the addition of cAMP pulses (arrows), fixed, and imaged by confocal microscopy.
(H) Schematic depiction of the presumptive localization of Hbx5 (green) in *crac*$^-$ cells in the absence or presence of cAMP pulses (blue boxes).
(I–K) Confocal images (I) and quantification (J and K) of TD uptake in *crac*$^-$ cells grown in HL5 (no starve) or developed for 6 h without or with cAMP pulses applied at different intervals. The plot in (J) shows data points with means and SD from one representative experiment; $n \geq 40$ for all conditions (n represents the number of cells analyzed). The plot in (K) shows normalized macropinocytic activity; mean and SD; n = 3 (n represents the number of experiments analyzed).
(L) Relative normalized expression of *gp80*, *phaps*, *hgsA*, and *pldY* in *crac*$^-$ cells that were developed without or with cAMP pulses applied at different intervals. Data represent mean + SEM; n = 3 (n represents the number of experiments analyzed).
Significance was determined by two-tailed unpaired t test in (E) and (F) and one-way ANOVA in (J) and (K). Scale bars: 5 μm in (B), (D), (G), and (I). AUs, arbitrary units in (E), (F), (J). and (K).

Please cite this article in press as: Hao et al., A transcription factor complex in *Dictyostelium* enables adaptive changes in macropinocytosis during the growth-to-development transition, Developmental Cell (2024), https://doi.org/10.1016/j.devcel.2024.01.012

In conclusion, our study provides fresh insights into the long-standing question of how *Dictyostelium* cells regulate macropinocytosis during growth and the transition to development. Similar to *Dictyostelium*, other cell types need to modulate macropinocytic activity in response to changing environmental conditions or for coordination with other cellular functions.[20,43] Moreover, oscillations at different spatiotemporal scales are increasingly being observed in biological systems and are often associated with the control of gene expression.[44] It will be of great interest in future studies to investigate whether similar mechanisms operate in other contexts to achieve coordinated regulation of macropinocytic activity among populations of cell or in response to repeated experience.

Limitations of the study

There remain unanswered questions regarding the function and regulation of Hbx5 and MybG. The precise mechanism by which Hbx5 and MybG form a complex to regulate transcription remains to be solved. Future studies are needed to elucidate how target genes of the Hbx5-MybG complex collectively control macropinocytosis and whether they function as conserved elements in higher eukaryotic cells. The signaling pathway responsible for transducing oscillatory cAMP signals to control nucleocytoplasmic shuttling of the Hbx5-MybG complex through protein phosphorylation and dephosphorylation has yet to be determined. Furthermore, Hbx5 and MybG likely regulate other cellular processes besides macropinocytosis, as evidenced by the fact that the DBD of Hbx5 is not required for the regulation of macropinocytosis, only a fraction of MybG binds and shuttles with Hbx5, and the deletion of *hbx5* and *mybG* have varying effects on multicellular development (Figures S1E and S2F). Further investigations are necessary to determine the other cellular functions regulated by Hbx5 and MybG and how these activities coordinate with macropinocytosis.

STAR★METHODS

Detailed methods are provided in the online version of this paper and include the following:

- KEY RESOURCES TABLE
- RESOURCE AVAILABILITY
  - Lead contact
  - Materials availability
  - Data and code availability
- EXPERIMENTAL MODEL AND STUDY PARTICIPANT DETAILS
  - Cell lines and cell culture
- METHOD DETAILS
  - Plasmid construction
  - Imaging
  - Macropinocytosis assay
  - Phagocytosis assay
  - Motility assay
  - Immunoprecipitation assay and mass spectrometry analysis
  - Immunoblotting
  - Phalloidin staining
  - RT-qPCR
  - Whole-transcriptome RNA-Seq
  - ChIP-seq
- QUANTIFICATION AND STATISTICAL ANALYSIS
  - Quantification
  - Statistical analysis

SUPPLEMENTAL INFORMATION

Supplemental information can be found online at https://doi.org/10.1016/j.devcel.2024.01.012.

ACKNOWLEDGMENTS

The authors thank Drs. Jeffrey A. Hadwiger (Oklahoma State University, USA), Peter N. Devreotes (Johns Hopkins University, USA), Robert R. Kay (MRC Laboratory of Molecular Biology, UK), and Masahiro Ueda (Osaka University, Japan) for providing cell lines and plasmids; Drs. Xiaozeng Yang and Yang Deng (Beijing Agro-Biotechnology Research Center) for help with bioinformatics analysis; the proteomics core facility in Peking University for MS analysis; Junying Jia, Shu Meng, and Ya Wang (Core Facility, Institute of Biophysics, CAS) for technical support in flow-cytometry experiments and high-content imaging; and Yan Teng (Center for Biological Imaging, Institute of Biophysics, CAS) for help with confocal imaging. This work was supported by grants from the Ministry of Science and Technology of China (2021YFA1300301 to H.C.), the Strategic Priority Research Program of CAS (XDB37020304 to H.C)., the National Natural Science Foundation of China (92254303 and 32170701 to H.C., 32370368 to L.L., 32270743 to Yihong Yang, and 12272202 to B.L.), the Beijing Natural Science Foundation (5234029 to H.T.), and the National Laboratory of Biomacromolecules.

AUTHOR CONTRIBUTIONS

Y.H., Yihong Yang, and H.T. performed most of the experiments and prepared the manuscript. Z.G. and L.L. conducted bioinformatics analyses. P.C. and B.L. performed image analyses. X.C., Y. Yuan, Z.W., X.M., S.Z., D.L., and Yanzhi Yang collected data. C.W. provided essential resources. H.C. and L.L. conceived and supervised the project and wrote the manuscript with contributions from other authors.

DECLARATION OF INTERESTS

The authors declare no competing interests.

Received: June 14, 2023
Revised: November 14, 2023
Accepted: January 17, 2024
Published: February 6, 2024

REFERENCES

1. Kay, R.R., Lutton, J., Coker, H., Paschke, P., King, J.S., and Bretschneider, T. (2022). The Amoebal Model for Macropinocytosis. Subcell. Biochem. *98*, 41–59.
2. Mylvaganam, S., Freeman, S.A., and Grinstein, S. (2021). The cytoskeleton in phagocytosis and macropinocytosis. Curr. Biol. *31*, R619–R632.
3. Swanson, J.A. (2008). Shaping cups into phagosomes and macropinosomes. Nat. Rev. Mol. Cell Biol. *9*, 639–649.
4. Buckley, C.M., and King, J.S. (2017). Drinking problems: mechanisms of macropinosome formation and maturation. FEBS Journal *284*, 3778–3790.
5. Donaldson, J.G. (2019). Macropinosome formation, maturation and membrane recycling: lessons from clathrin-independent endosomal membrane systems. Philos. Trans. R. Soc. Lond. B Biol. Sci. *374*, 20180148.
6. Swanson, J.A., and King, J.S. (2019). The breadth of macropinocytosis research. Philos. Trans. R. Soc. Lond. B Biol. Sci. *374*, 20180146.

Please cite this article in press as: Hao et al., A transcription factor complex in *Dictyostelium* enables adaptive changes in macropinocytosis during the growth-to-development transition, Developmental Cell (2024), https://doi.org/10.1016/j.devcel.2024.01.012

7. Lin, X.P., Mintern, J.D., and Gleeson, P.A. (2020). Macropinocytosis in Different Cell Types: Similarities and Differences. Membranes *10*, 177.
8. Hacker, U., Albrecht, R., and Maniak, M. (1997). Fluid-phase uptake by macropinocytosis in Dictyostelium. J. Cell Sci. *110*, 105–112.
9. Le, A.H., Yelland, T., Paul, N.R., Fort, L., Nikolaou, S., Ismail, S., and Machesky, L.M. (2021). CYRI-A limits invasive migration through macropinosome formation and integrin uptake regulation. J. Cell Biol. *220*, e202012114.
10. Shao, X., Cao, G., Chen, D., Liu, J., Yu, B., Liu, M., Li, Y.X., Cao, B., Sadovsky, Y., and Wang, Y.L. (2021). Placental trophoblast syncytialization potentiates macropinocytosis via mTOR signaling to adapt to reduced amino acid supply. Proc. Natl. Acad. Sci. USA *118*. e2017092118.
11. Moreau, H.D., Blanch-Mercader, C., Attia, R., Maurin, M., Alraies, Z., Sanséau, D., Malbec, O., Delgado, M.G., Bousso, P., Joanny, J.F., et al. (2019). Macropinocytosis Overcomes Directional Bias in Dendritic Cells Due to Hydraulic Resistance and Facilitates Space Exploration. Dev. Cell *49*, 171–188.e5.
12. Saeed, M.F., Kolokoltsov, A.A., Albrecht, T., and Davey, R.A. (2010). Cellular entry of ebola virus involves uptake by a macropinocytosis-like mechanism and subsequent trafficking through early and late endosomes. PLoS Pathog. *6*, e1001110.
13. Commisso, C., Davidson, S.M., Soydaner-Azeloglu, R.G., Parker, S.J., Kamphorst, J.J., Hackett, S., Grabocka, E., Nofal, M., Drebin, J.A., Thompson, C.B., et al. (2013). Macropinocytosis of protein is an amino acid supply route in Ras-transformed cells. Nature *497*, 633–637.
14. Palm, W., Park, Y., Wright, K., Pavlova, N.N., Tuveson, D.A., and Thompson, C.B. (2015). The Utilization of Extracellular Proteins as Nutrients Is Suppressed by mTORC1. Cell *162*, 259–270.
15. Wyant, G.A., Abu-Remaileh, M., Wolfson, R.L., Chen, W.W., Freinkman, E., Danai, L.V., Vander Heiden, M.G., and Sabatini, D.M. (2017). mTORC1 Activator SLC38A9 Is Required to Efflux Essential Amino Acids from Lysosomes and Use Protein as a Nutrient. Cell *171*, 642–654.e12.
16. Kim, S.M., Nguyen, T.T., Ravi, A., Kubiniok, P., Finicle, B.T., Jayashankar, V., Malacrida, L., Hou, J., Robertson, J., Gao, D., et al. (2018). PTEN Deficiency and AMPK Activation Promote Nutrient Scavenging and Anabolism in Prostate Cancer Cells. Cancer Discov. *8*, 866–883.
17. Ramirez, C., Hauser, A.D., Vucic, E.A., and Bar-Sagi, D. (2019). Plasma membrane V-ATPase controls oncogenic RAS-induced macropinocytosis. Nature *576*, 477–481.
18. Yao, W., Rose, J.L., Wang, W., Seth, S., Jiang, H., Taguchi, A., Liu, J., Yan, L., Kapoor, A., Hou, P., et al. (2019). Syndecan 1 is a critical mediator of macropinocytosis in pancreatic cancer. Nature *568*, 410–414.
19. Canton, J., Schlam, D., Breuer, C., Gütschow, M., Glogauer, M., and Grinstein, S. (2016). Calcium-sensing receptors signal constitutive macropinocytosis and facilitate the uptake of NOD2 ligands in macrophages. Nat. Commun. *7*, 11284.
20. Lambies, G., and Commisso, C. (2022). Macropinocytosis and Cancer: From Tumor Stress to Signaling Pathways. Subcell. Biochem. *98*, 15–40.
21. Lee, S.W., Zhang, Y., Jung, M., Cruz, N., Alas, B., and Commisso, C. (2019). EGFR-Pak Signaling Selectively Regulates Glutamine Deprivation-Induced Macropinocytosis. Dev. Cell *50*, 381–392.e5.
22. King, B., Araki, J., Palm, W., and Thompson, C.B. (2020). Yap/Taz promote the scavenging of extracellular nutrients through macropinocytosis. Genes Dev. *34*, 1345–1358.
23. Mendel, Z.I., Reynolds, M.B., Abuaita, B.H., O'Riordan, M.X., and Swanson, J.A. (2022). Amino acids suppress macropinocytosis and promote release of CSF1 receptor in macrophages. J. Cell Sci. *135*, jcs259284.
24. Bloomfield, G., Traynor, D., Sander, S.P., Veltman, D.M., Pachebat, J.A., and Kay, R.R. (2015). Neurofibromin controls macropinocytosis and phagocytosis in Dictyostelium. eLife *4*, e04940.
25. Tomchik, K.J., and Devreotes, P.N. (1981). Adenosine 3′,5′-monophosphate waves in Dictyostelium discoideum: a demonstration by isotope dilution–fluorography. Science *212*, 443–446.
26. Maeda, M., Lu, S., Shaulsky, G., Miyazaki, Y., Kuwayama, H., Tanaka, Y., Kuspa, A., and Loomis, W.F. (2004). Periodic signaling controlled by an oscillatory circuit that includes protein kinases ERK2 and PKA. Science *304*, 875–878.
27. Gregor, T., Fujimoto, K., Masaki, N., and Sawai, S. (2010). The onset of collective behavior in social amoebae. Science *328*, 1021–1025.
28. Katoh, M., Chen, G., Roberge, E., Shaulsky, G., and Kuspa, A. (2007). Developmental commitment in Dictyostelium discoideum. Eukaryot. Cell *6*, 2038–2045.
29. Williams, T.D., and Kay, R.R. (2018). The physiological regulation of macropinocytosis during Dictyostelium growth and development. J. Cell Sci. *131*.
30. Maeda, Y. (1983). Axenic Growth of Dictyostelium Discoideum Wild-Type Nc-4 Cells and Its Relation to Endocytotic Ability. Microbiology *129*, 2467–2473.
31. Zhang, Y., Tu, H., Hao, Y., Li, D., Yang, Y., Yuan, Y., Guo, Z., Li, L., Wang, H., and Cai, H. (2022). Oligopeptide transporter Slc15A modulates macropinocytosis in Dictyostelium by maintaining intracellular nutrient status. J. Cell Sci. *135*, jcs259450.
32. Veltman, D.M., Williams, T.D., Bloomfield, G., Chen, B.C., Betzig, E., Insall, R.H., and Kay, R.R. (2016). A plasma membrane template for macropinocytic cups. eLife *5*, e20085.
33. Maekawa, M., Terasaka, S., Mochizuki, Y., Kawai, K., Ikeda, Y., Araki, N., Skolnik, E.Y., Taguchi, T., and Arai, H. (2014). Sequential breakdown of 3-phosphorylated phosphoinositides is essential for the completion of macropinocytosis. Proc. Natl. Acad. Sci. USA *111*, E978–E987.
34. Tu, H., Wang, Z., Yuan, Y., Miao, X., Li, D., Guo, H., Yang, Y., and Cai, H. (2022). The PripA-TbcrA complex-centered Rab GAP cascade facilitates macropinosome maturation in Dictyostelium. Nat. Commun. *13*, 1787.
35. Singer, G., Araki, T., and Weijer, C.J. (2019). Oscillatory cAMP cell-cell signalling persists during multicellular Dictyostelium development. Commun. Biol. *2*, 139.
36. Cai, H., Katoh-Kurasawa, M., Muramoto, T., Santhanam, B., Long, Y., Li, L., Ueda, M., Iglesias, P.A., Shaulsky, G., and Devreotes, P.N. (2014). Nucleocytoplasmic shuttling of a GATA transcription factor functions as a development timer. Science *343*, 1249531.
37. Hashimura, H., Morimoto, Y.V., Yasui, M., and Ueda, M. (2019). Collective cell migration of Dictyostelium without cAMP oscillations at multicellular stages. Commun. Biol. *2*, 34.
38. Hadwiger, J.A., Cai, H., Aranda, R.G., and Fatima, S. (2022). An atypical MAPK regulates translocation of a GATA transcription factor in response to chemoattractant stimulation. J. Cell Sci. *135*, jcs260148.
39. Nichols, J.M.E., Paschke, P., Peak-Chew, S., Williams, T.D., Tweedy, L., Skehel, M., Stephens, E., Chubb, J.R., and Kay, R.R. (2019). The Atypical MAP Kinase ErkB Transmits Distinct Chemotactic Signals through a Core Signaling Module. Dev. Cell *48*, 491–505.e9.
40. Insall, R., Kuspa, A., Lilly, P.J., Shaulsky, G., Levin, L.R., Loomis, W.F., and Devreotes, P. (1994). CRAC, a cytosolic protein containing a pleckstrin homology domain, is required for receptor and G protein-mediated activation of adenylyl cyclase in Dictyostelium. J. Cell Biol. *126*, 1537–1545.
41. Veltman, D.M., Lemieux, M.G., Knecht, D.A., and Insall, R.H. (2014). PIP_3-dependent macropinocytosis is incompatible with chemotaxis. J. Cell Biol. *204*, 497–505.
42. Santhanam, B., Cai, H., Devreotes, P.N., Shaulsky, G., and Katoh-Kurasawa, M. (2015). The GATA transcription factor GtaC regulates early developmental gene expression dynamics in Dictyostelium. Nat. Commun. *6*, 7551.
43. Delgado, M.G., Rivera, C.A., and Lennon-Duménil, A.M. (2022). Macropinocytosis and Cell Migration: Don't Drink and Drive…. Subcell. Biochem. *98*, 85–102.
44. Venkatachalam, V., Jambhekar, A., and Lahav, G. (2022). Reading oscillatory instructions: How cells achieve time-dependent responses to oscillating transcription factors. Curr. Opin. Cell Biol. *77*, 102099.

Please cite this article in press as: Hao et al., A transcription factor complex in *Dictyostelium* enables adaptive changes in macropinocytosis during the growth-to-development transition, Developmental Cell (2024), https://doi.org/10.1016/j.devcel.2024.01.012

45. Yang, Y., Li, D., Chao, X., Singh, S.P., Thomason, P., Yan, Y., Dong, M., Li, L., Insall, R.H., and Cai, H. (2021). Leep1 interacts with PIP3 and the Scar/WAVE complex to regulate cell migration and macropinocytosis. J. Cell Biol. *220*, e202010096.

46. Li, D., Yang, Y., Lv, C., Wang, Y., Chao, X., Huang, J., Singh, S.P., Yuan, Y., Zhang, C., Lou, J., et al. (2023). GxcM-Fbp17/RacC-WASP signaling regulates polarized cortex assembly in migrating cells via Arp2/3. J. Cell Biol. *222*, e202208151.

47. Cai, H., Huang, C.H., Devreotes, P.N., and Iijima, M. (2012). Analysis of chemotaxis in Dictyostelium. Methods Mol. Biol. *757*, 451–468.

48. Paschke, P., Knecht, D.A., Silale, A., Traynor, D., Williams, T.D., Thomason, P.A., Insall, R.H., Chubb, J.R., Kay, R.R., and Veltman, D.M. (2018). Rapid and efficient genetic engineering of both wild type and axenic strains of Dictyostelium discoideum. PLoS One *13*, e0196809.

49. Veltman, D.M., Keizer-Gunnink, I., and Haastert, P.J. (2009). An extrachromosomal, inducible expression system for Dictyostelium discoideum. Plasmid *61*, 119–125.

50. Cai, H., Das, S., Kamimura, Y., Long, Y., Parent, C.A., and Devreotes, P.N. (2010). Ras-mediated activation of the TORC2-PKB pathway is critical for chemotaxis. J. Cell Biol. *190*, 233–245.

51. Wingett, S.W., and Andrews, S. (2018). FastQ Screen: A tool for multi-genome mapping and quality control. F1000Res *7*, 1338.

52. Langmead, B., and Salzberg, S.L. (2012). Fast gapped-read alignment with Bowtie 2. Nat. Methods *9*, 357–359.

53. Pertea, M., Kim, D., Pertea, G.M., Leek, J.T., and Salzberg, S.L. (2016). Transcript-level expression analysis of RNA-seq experiments with HISAT, StringTie and Ballgown. Nat. Protoc. *11*, 1650–1667.

54. Love, M.I., Huber, W., and Anders, S. (2014). Moderated estimation of fold change and dispersion for RNA-seq data with DESeq2. Genome Biol. *15*, 550.

55. Maere, S., Heymans, K., and Kuiper, M. (2005). BiNGO: a Cytoscape plugin to assess overrepresentation of gene ontology categories in biological networks. Bioinformatics *21*, 3448–3449.

56. Zhang, Y., Liu, T., Meyer, C.A., Eeckhoute, J., Johnson, D.S., Bernstein, B.E., Nusbaum, C., Myers, R.M., Brown, M., Li, W., et al. (2008). Model-based analysis of ChIP-Seq (MACS). Genome Biol. *9*, R137.

Please cite this article in press as: Hao et al., A transcription factor complex in *Dictyostelium* enables adaptive changes in macropinocytosis during the growth-to-development transition, Developmental Cell (2024), https://doi.org/10.1016/j.devcel.2024.01.012

STAR★METHODS

KEY RESOURCES TABLE

REAGENT or RESOURCE	SOURCE	IDENTIFIER
Antibodies		
Anti-GFP antibody	Roche	Cat# 11814460001; RRID: AB_390913
Anti-DsRed antibody	TaKaRa	Cat# 632496; RRID: AB_10013483
Anti-Phospho-Thr/Tyr antibody	Cell Signaling Technology	Cat# 9381; RRID: AB_330301
Anti-Phospho-p44/42 MAPK antibody	Cell Signaling Technology	Cat# 4370; RRID: AB_2315112
Anti-GFP antibody	Abcam	Cat# ab290; RRID: AB_303395
Bacterial and virus strains		
E.coli strain XL1-Blue	Peter Devreotes laboratory (Johns Hopkins University, USA)	N/A
GST-GFP expressing *E.coli strain*	Tu et al.[34]	N/A
Klebsiella aerogenes	Peter Devreotes laboratory (Johns Hopkins University, USA)	N/A
Chemicals, peptides, and recombinant proteins		
T4 DNA Ligase	NEB	Cat# M0202V
G418	Thermo Fisher Scientific	Cat# 10131035
Hygromycin B	Thermo Fisher Scientific	Cat# 10687010
Blasticidin S	Sigma	Cat# 3513-03-9
Adenosine 3′,5′-cyclic monophosphate sodium salt monohydrate	Sigma	Cat# A6885
Folic acid	Sigma	Cat# F7876
EDTA-free protease inhibitor cocktail	Roche	Cat# 11836170001
λ-phosphatase	NEB	Cat# P0753S
Phosphatase buffer	NEB	Cat# P0753
Sodium orthovanadate	NEB	Cat# P0758L
Sodium Pyrophosphate	Sigma	Cat# 221368
Proteinase K	Roche	Cat# 3115879001
RNase A	Merck	Cat# RNASEA-RO
Formaldehyde	NOVON	Cat# SS2097
Glutaraldehyde	Sigma	Cat# G7651
Acti-Stain 555 Phalloidin	Cytoskeleton	Cat# PHDH1
Trizol	Invitrogen	Cat# 15596018
70 kDa TRITC-dextran	Sigma	Cat# T1162
70 kDa FITC-dextran	Sigma	Cat# 46945
DQ-BSA	Invitrogen	Cat# D-12050
Alexa 647-BSA	Invitrogen	Cat# A34785
pHrodo Red	Invitrogen	Cat# P36600
Critical commercial assays		
Phusion High-Fidelity PCR Master Mix	NEB	Cat# M0532L
ECL™ Direct Nucleic Acid Labeling And Detection Systems	Cytiva	Cat# RPN3001
gDNA Eraser	TaKaRa	Cat# RR047B
PrimeScript RT reagent kit	TaKaRa	Cat# RR047A
TB Green Fast qPCR Mix	TaKaRa	Cat# RR430A
TIANprep rapid mini plasmid kit	TIANGEN	Cat# DP05-02

(*Continued on next page*)

Please cite this article in press as: Hao et al., A transcription factor complex in *Dictyostelium* enables adaptive changes in macropinocytosis during the growth-to-development transition, Developmental Cell (2024), https://doi.org/10.1016/j.devcel.2024.01.012

Continued

REAGENT or RESOURCE	SOURCE	IDENTIFIER
Deposited data		
ChIP-seq and RNA-seq analyses of Hbx5-MybG target genes	This paper, Sequence Read Archive database	PRJNA972516
Mass spectrometry analysis of Hbx5 immunoprecipitation	This paper, ProteomeXchange Consortium	PXD046585
Experimental models: Cell lines		
Dictyostelium discoideum AX2 cell line	Robert Kay laboratory (MRC Laboratory of Molecular Biology, UK)	DBS0235521
Dictyostelium discoideum crac^{-} cell line	Peter Devreotes laboratory (Johns Hopkins University, USA)	N/A
Dictyostelium discoideum car1^{-}*3*$^{-}$ cell line	Peter Devreotes laboratory (Johns Hopkins University, USA)	N/A
Dictyostelium discoideum erkB^{-} cell line	Jeffrey Hadwiger laboratory (Oklahoma State University, USA)	N/A
Dictyostelium discoideum hbx5 REMI mutant cell line	This paper	N/A
Dictyostelium discoideum hbx5^{-} cell line	This paper	N/A
Dictyostelium discoideum mybG^{-} cell line	This paper	N/A
Dictyostelium discoideum hgsA^{-}*hgsB*$^{-}$ cell line	This paper	N/A
Dictyostelium discoideum phaps^{-} cell line	This paper	N/A
Dictyostelium discoideum pldY^{-} cell line	This paper	N/A
Dictyostelium discoideum rasW/V/X/Y^{-} cell line	This paper	N/A
Dictyostelium discoideum hbx5-GFP knock-in cell line	This paper	N/A
Dictyostelium discoideum mybG-GFP knock-in cell line	This paper	N/A
Oligonucleotides		
Primers for RT-qPCR	This paper	Summarized in Table S3
Primers for generation of expression constructs	This paper	Summarized in Table S3
Primers for generation of knockout cells	This paper	Summarized in Table S3
Primers for generation of GFP knock-in cells	This paper	Summarized in Table S3
Recombinant DNA		
pDM317 GFP-Hbx5	This paper	N/A
pDM323 Hbx5-GFP	This paper	N/A
pBlueScript Hbx5$^{\Delta DBD}$	This paper	N/A
pDM323 Hbx5$^{\Delta DBD}$-GFP	This paper	N/A
pDM323 Hbx5^{N1}-GFP	This paper	N/A
pDM317 GFP-Hbx5^{N2}	This paper	N/A
pDM317 GFP-Hbx5^{N3}	This paper	N/A
pDM323 Hbx5^{C1}-GFP	This paper	N/A
pDM323 Hbx5^{C2}-GFP	This paper	N/A
pDM323 Hbx5^{M}-GFP	This paper	N/A
pDM323 Hbx5^{N2}-NES-GFP	This paper	N/A
pDM304 NLS-GFP	This paper	N/A
pDM323 NLS-Hbx5^{N2}-GFP	This paper	N/A
pDM323 NLS-Hbx5^{N3}-GFP	This paper	N/A
pDM317 GFP-MybG	This paper	N/A
pDM323 MybG-GFP	This paper	N/A

(*Continued on next page*)

Please cite this article in press as: Hao et al., A transcription factor complex in *Dictyostelium* enables adaptive changes in macropinocytosis during the growth-to-development transition, Developmental Cell (2024), https://doi.org/10.1016/j.devcel.2024.01.012

Continued

REAGENT or RESOURCE	SOURCE	IDENTIFIER
pEASY MybG$^{\Delta DBD}$	This paper	N/A
pDM323 MybG$^{\Delta DBD}$-GFP	This paper	N/A
pDM323 MybG^{C1}-GFP	This paper	N/A
pDM317 GFP-MybG^{N1}	This paper	N/A
pDM317 GFP-MybG^{N2}	This paper	N/A
pDM317 GFP-MybG^{N3}	This paper	N/A
pDM451 MybG-RFP	This paper	N/A
pDM451 MybG^{C1}-RFP	This paper	N/A
pDM449 RFP-MybG^{N2}	This paper	N/A
pDM449 RFP-MybG^{N3}	This paper	N/A
pDM324 H2Bv3-RFP	This paper	N/A
pDM451 H2Bv3-RFP	This paper	N/A
pDM323 NLS-Hbx5-GFP	This paper	N/A
pDM323 2×NLS-Hbx5-GFP	This paper	N/A
pB18 2×NLS-Hbx5-GFP	This paper	N/A
pDM317 GFP-DydA	This paper	N/A
pDM449 RFP-DydA	This paper	N/A
pDM317 GFP-DDB_G0284825	This paper	N/A
pDM451 MybG-NES-RFP	This paper	N/A
GFP-Rab5A	Tu et al.[34]	N/A
GFP-Rab7A	Tu et al.[34]	N/A
TAPP1-RFP	Tu et al.[34]	N/A
GFP-2×FYVE	Tu et al.[34]	N/A
PHcrac-GFP	Peter Devreotes laboratory (Johns Hopkins University, USA)	N/A
LimEΔcoil-GFP	Peter Devreotes laboratory (Johns Hopkins University, USA)	N/A
GFP-RBD	Peter Devreotes laboratory (Johns Hopkins University, USA)	N/A
Flamindo2	Masahiro Ueda laboratory (Osaka University, Japan)	N/A
Software and algorithms		
NIH ImageJ	NIH Image	https://imagej.net/ij/
Fiji ImageJ	Open-source platform	https://imagej.net/software/fiji/
Prism 9.0	GraphPad Software	https://www.graphpad.com
ZEN	ZEISS	https://www.zeiss.com/
FlowJo	Tree star software	https://www.flowjo.com/
Ibidi chemotaxis tool software	Ibidi	https://ibidi.com/chemotaxis-analysis/171-chemotaxis-and-migration-tool.html
Other		
2-well coverslip chamber	Thermo Fisher Scientific	Cat# 154461PK
8-well coverslip chamber	Thermo Fisher Scientific	Cat# 154534PK
35 mm glass-bottom dish	Corning	Cat# 430165
HL5 medium	Formedium	Cat# HLF3
LoFlo medium	Formedium	Cat# LFG0501
SM Agar	Formedium	Cat# SMA0102
Anti-GFP affinity beads	Smart Lifesciences	Cat# SA070005
Anti-RFP affinity beads	Smart Lifesciences	Cat# SA072005
Protein G Dynabeads	Invitrogen	Cat# 10007D
SeaKem GTG agarose	Lonza	Cat# 50070

Please cite this article in press as: Hao et al., A transcription factor complex in *Dictyostelium* enables adaptive changes in macropinocytosis during the growth-to-development transition, Developmental Cell (2024), https://doi.org/10.1016/j.devcel.2024.01.012

RESOURCE AVAILABILITY

Lead contact

Further information and requests for resources and reagents should be directed to and will be fulfilled by the lead contact, Huaqing Cai (huaqingcai@ibp.ac.cn).

Materials availability

All unique reagents and plasmids reported in this paper are available from the lead contact upon request.

Data and code availability

- The RNA-seq data and ChIP-seq data were deposited into the Sequence Read Archive database. The mass spectrometry proteomics data were deposited to the ProteomeXchange Consortium. Accession numbers are listed in the key resources table.
- The code for analyzing the nucleocytoplasmic shuttling of the transcription factors and the temporal auto-correlation is available from the lead contact upon request.
- Any additional information required to reanalyze the data reported in this paper is available from the lead contact upon request.

EXPERIMENTAL MODEL AND STUDY PARTICIPANT DETAILS

Cell lines and cell culture

WT cells were derived from the Ax2 (Ka) axenic strain of *Dictyostelium discoideum* provided by Robert Kay laboratory (MRC Laboratory of Molecular Biology, UK). REMI screen was performed as described previously.[31] The *hbx5* REMI mutant contains an insertion of the Blasticidin S resistance (BSR) cassette at position 2,037 (numbered from the ATG translation start site) of the *hbx5* genomic locus. *crac*$^{-}$ and *car1*$^{-}$*3*$^{-}$ cells were obtained from Peter Devreotes laboratory (Johns Hopkins University, USA). *erkB*$^{-}$ cells were obtained from Jeffrey Hadwiger laboratory (Oklahoma State University, USA). All the other knockout cell lines were generated in Ax2. Hbx5-GFP knock-in cell line was generated in Ax2. MybG-GFP knock-in cell lines were generated in Ax2 and *hbx5*$^{-}$. Cells stably expressing 2×NLS-Hbx5-GFP were selected after single cell expansion with bacteria. At least two independent clones were selected for each knockout, knock-in, or stable cell line. Their phenotypes were compared, and results from one representative clone are shown. Cells were routinely cultured in HL5 medium (Formedium) supplemented with antibiotics at 22°C. Cells carrying expression constructs were maintained in HL5 containing G418 (10 to 20 μg/mL), Hygromycin (50 μg/mL), or Blasticidin S (10 μg/mL). Growth and development on bacteria (*Klebsiella aerogenes*) lawn were performed as described previously.[31]

METHOD DETAILS

Plasmid construction

Plasmids and primers used in this study are listed in key resources table and Table S3. PHcrac-GFP, LimEΔcoil-GFP, GFP-Rab5A, GFP-Rab7A, TAPP1-RFP, GFP-2×FYVE, GFP-RBD, and Flamindo2 were described previously.[34,37,45–47] To make knockout constructs for gene deletion, 5' and 3' arms were PCR-amplified from genomic DNA and cloned upstream and downstream of a BSR cassette or a Hygromycin resistance cassette,[48] respectively. The resulting disruption cassette was PCR-amplified or digested from the knockout construct and electroporated into cells. Gene disruption was confirmed by resistance to Blasticidin or Hygromycin, PCR, and Southern blot. Hbx5-GFP and MybG-GFP knock-in cells were generated by replacing the region of *hbx5* between +5,483 and +6,034 and the region of *mybG* between +1,409 and +1,534 with a GFP-hygromycin cassette from pDM1355,[48] respectively. Knock-in clones were selected by resistance to hygromycin and confirmed by PCR and Western blot.

To generate constructs expressing GFP- or RFP-fused proteins, DNA fragments were PCR-amplified and cloned into *Dictyostelium* expression vectors[49] containing a multiple cloning site. To generate Hbx5$^{\Delta DBD}$-GFP and MybG$^{\Delta DBD}$-GFP, Hbx5 and MybG were first cloned into pBlueScript and pEASY, respectively. Hbx5 and MybG deleted of the DBD were then used as templates for PCR amplification and the resulting DNA fragments were cloned into pDM323. To generate Hbx5^{N2}-NES-GFP and MybG-NES-RFP, reverse primers containing the NES sequence were used for PCR amplification. To generate NLS-GFP, NLS-Hbx5-GFP, NLS-Hbx5^{N2}-GFP, and NLS-Hbx5^{N3}-GFP, forward primers containing an NLS sequence were used for PCR amplification. To generate 2×NLS-Hbx5-GFP, NLS-Hbx5-GFP was used as the template for another round of PCR amplification to add the second NLS sequence and the PCR product was cloned into pDM323 or pB18 expression vectors containing a multiple cloning site.

Imaging

All images were taken on a Zeiss 880 inverted microscope using a 63 ×/1.4 oil-immersion objective or a 40×/0.95 oil-immersion objective at room temperature.

For experiments presented in Figures 1H, 2F, S3, S5A, S8A, and S8C–S8G, 10^5 cells were plated in 8-well coverslip chamber (Lab-Tek, NalgenNunc) and allowed to adhere before imaging.

For experiments presented in Figures 5A, 6A, 6E, S5B, S6, S7A, and S8B, cells were plated in 2-well coverslip chamber at a density of 2 × 10^6 cells/well and submerged in development buffer (DB; 5 mM Na_2HPO_4, 5 mM KH_2PO_4, 2 mM Mg_2SO_4, 0.2 mM $CaCl_2$, pH

Please cite this article in press as: Hao et al., A transcription factor complex in *Dictyostelium* enables adaptive changes in macropinocytosis during the growth-to-development transition, Developmental Cell (2024), https://doi.org/10.1016/j.devcel.2024.01.012

6.5). Time-lapse images were acquired when periodic movement of cells was observed during early development or when the cells had entered the streaming stage.

For cAMP stimulation experiments presented in Figures 5E–5H, 6I, 6J, and 7B, cells were developed with cAMP pulses as described previously.[36] In brief, cells were washed with DB, starved in DB for 1 h at 2×10^7 cells/mL, and then pulsed with 50-100 nM cAMP for 3-4 h. 450 μL of developed cells at a density of 2×10^5 cells/mL were plated in 8-well cover slip chamber. Cells were allowed to adhere. 50 μL of 10 μM cAMP was added for stimulation. For the removal of cAMP, the stimulus was applied for 5 min for the nuclear-to-cytoplasmic translocation to complete, and imaging was then started when the stimulus was replaced with DB.

For folic acid stimulation experiment presented in Figure S7C, 10^5 vegetative cells were plated in 8-well coverslip chamber. After the cells settled, HL5 was replaced with DB for about 30 min. Folic acid of 500 μM was then added for stimulation.

For experiments presented in Figures 7G and S9A, *crac*$^-$ cells expressing Hbx5-GFP were starved in DB for 2 h at 2×10^7 cells/mL, and then pulsed with 50 nM cAMP applied at different intervals for 4 h. Cells were collected before or at different time points after the addition of one pulse of cAMP (50 nM) and fixed immediately in KK2 (6.5 mM KH_2PO_4, 3.8 mM K_2HPO_4, pH 6.2) containing 2% formaldehyde and 0.8% glutaraldehyde. Fixed cells were plated on chambered cover slip. Images were acquired after cells attached. For experiments presented in Figures 5J, S7F, and S7G, WT cells expressing Hbx5-GFP or Hbx5^M-GFP were starved in DB for 1 h at 2×10^7 cells/mL, and then pulsed with 50-100 nM cAMP applied at 6-min intervals for 2 h. The cells were then stimulated with cAMP at 6-min or 3-min intervals. After 18 min, cells were collected before or at different time points after the addition of one pulse of cAMP, fixed, and imaged as described above.

Macropinocytosis assay

For experiments presented in Figures 1A, 1J, 2B, 2J, 3B, 3E, 4C, 4G, and S1A, cells were incubated in HL5 medium containing 0.5 mg/mL TD (Sigma) for 30-60 min.

For experiments presented in Figures 7D–7F, WT cells expressing Hbx5-GFP or 2×NLS-Hbx5-GFP were seeded in 8-well cover slip chamber at 3×10^5 cells/well in DB. At 0, 6, 8, and 10 h, cells were incubated with 0.5 mg/mL TD for 30 min. For experiments presented in Figures 7I–7K, *crac*$^-$ cells were used to measure macropinocytic activity. For the "no starve" and "no pulse" conditions, the cells were incubated in HL5 and DB, respectively. For the other conditions, the cells were starved in DB for 2 h at 2×10^7 cells/mL, and then pulsed with 50 nM cAMP applied at different intervals for 6 h. After these treatments, cells were incubated in DB containing 0.5 mg/mL TD for 30 min. To quantify TD uptake, the medial optical section of cell was imaged.

Macropinocytosis dynamics was recorded in cells expressing PHcrac-GFP by time-lapse imaging. The rate of macropinocytosis was quantified by tracking the number of membrane ruffles or enclosed macropinosomes formed in 5 min. Macropinosome size was determined by measuring the area of newly formed macropinosomes immediately after ruffle closure with the freehand line tool in ImageJ.

Fluorimetric analysis of macropinocytosis was performed as described previously.[31] In brief, cells shaken at a density of 5×10^6/mL in growth medium were incubated with 1 mg/mL TD. Aliquots of 300 μL of cells were taken at each time point and mixed briefly with Trypan Blue solution on ice. Cells were washed once with 1 mL ice-cold Sörensen buffer and resuspended in 0.5 mL Sörensen buffer. Fluorescence was measured using a Tecan Spark fluorescence spectrophotometer (544-nm excitation and 574-nm emission). Obtained values were normalized to protein content.

Flow cytometry analysis of macropinocytosis was performed as described previously.[34] In brief, $2\text{-}3\times10^6$ cells seeded in 6-well plate were incubated in HL5 supplemented with 0.5 mg/mL TD for 30 min. After incubation, cells were washed with ice-cold KK2 buffer containing 10 mM EDTA and resuspended in KK2 containing 5 mM sodium azide. The total fluorescence intensity per cell was determined by a BD Biosciences Influx flow cytometer and data were analyzed by FlowJo_v10.8.1.

To measure degradation along the macropinocytic pathway, cells were incubated in HL5 medium containing 20 μg/mL DQ-BSA (Invitrogen) and 100 μg/mL Alexa 647-BSA (Invitrogen) for 60 min. Fluorescence intensity was quantified by ImageJ (NIH) and normalized to cell area.

For experiments presented in Figures S9B and S9C, cells were grown in HL5 medium or suspensions of *Klebsiella aerogenes* at an optical density (OD_{600}) of 2.0 in SorMC buffer (15 mM KH_2PO_4, 2 mM Na_2HPO_4, 50 μM $MgCl_2$, 50 μM $CaCl_2$, pH 6.0). Cells were incubated with 0.5 mg/mL TD for 60 min before imaging. For experiments presented in Figures S9D and S9E, 5×10^5 cells were seeded in 35 mm glass-bottom dish in HL5 medium containing 0.5 mg/mL TD. The cells were overlaid with a thin sheet of agarose (0.5% SeaKem GTG agarose dissolved in LoFlo medium containing 0.5 mg/mL TD). The cells were allowed to internalize TD for 60 min before imaging.

Phagocytosis assay

For labelling of *Klebsiella aerogenes*, the bacteria were cultured in HL5 medium at a starting OD_{600} of 0.1. The bacteria were harvested at OD_{600} of 0.6, washed twice with phosphate-buffered saline (PBS), and incubated with 1 μM pHrodo Red (Invitrogen) in PBS at 1×10^9/mL. After a 15 min incubation at room temperature, the labeled bacteria were washed with PBS and resuspended in PBS at 1×10^9/mL. For flow cytometry analysis, 5 mL of cells were shaken at a density of 2×10^6/mL in Sörensen buffer (15 mM KH_2PO_4, 2 mM Na_2HPO_4, pH 6.0) containing 120 mM sorbitol for 15 min. Then, the cells were incubated with 5×10^8 labeled bacteria for 30 min. The cells were then washed with ice-cold Sörensen buffer containing 5 mM sodium azide and resuspended in basic buffer (50 mM Tris-HCl, 150 mM NaCl, pH 8.8). The total fluorescence intensity per cell was determined by a BD Biosciences Influx flow cytometer, and the data were analyzed using FlowJo_v10.8.1.

Please cite this article in press as: Hao et al., A transcription factor complex in *Dictyostelium* enables adaptive changes in macropinocytosis during the growth-to-development transition, Developmental Cell (2024), https://doi.org/10.1016/j.devcel.2024.01.012

The bacteria killing assay was performed as described previously.[34] In brief, GFP-expressing bacteria were resuspended in HL5 medium to a concentration 2×10^8/mL. Next, 10 μL of the bacteria culture in 400 μL of HL5 medium was added into 8-well coverslip chamber before the addition of 10^5 cells. Images were acquired every 14 s for a total of 100 frames.

Motility assay

Random motility assay was performed as described previously.[46] In brief, vegetative cells were seeded in HL5 medium and allowed to adhere for 4 h. Before imaging, the medium was replaced with fresh HL5 medium. Images were acquired with phase illumination on a Zeiss 880 inverted microscope equipped with a 10×/0.45 objective.

Immunoprecipitation assay and mass spectrometry analysis

To identify proteins that interact specifically with Hbx5, cells expressing NLS-GFP, NLS-Hbx5^{N3}-GFP, or NLS-Hbx5^{N2}-GFP were lysed by ice-cold lysis buffer [20 mM Hepes (pH 7.2), 50 mM NaCl, 0.5% NP40, 50 mM NaF, 25 mM sodium pyrophosphate, 2 mM Na_3VO_4, 5% glycerol and complete EDTA-free protease inhibitor cocktail (Roche)] and incubated for 5 min on ice. Lysates were centrifuged at 22,000 × g for 10 min at 4°C. The supernatants were incubated with anti-GFP affinity beads (Smart Lifesciences) for 1 h at 4°C. Beads were washed four times with lysis buffer. Samples were eluted with SDS loading buffer and subjected to SDS-PAGE. Each gel lane was divided into 4 slices and subjected to in-gel trypsin digestion and mass spectrometry analysis as described before.[45]

For co-IP experiments presented in Figures 2A, 3D, and 3G, cells were lysed as above. The supernatants were incubated with anti-GFP affinity beads or anti-RFP affinity beads (Smart Lifesciences) for 1.5 h at 4°C. Beads were washed four times with lysis buffer. Samples were eluted with SDS loading buffer and subjected to SDS-PAGE. Western blotting was carried out as described before.[50] Anti-GFP antibody (WB, 1:5000) was purchased from Roche. Anti-DsRed antibody (WB, 1:1000), which was used to detect RFP-fusion proteins, was purchased from TaKaRa.

Immunoblotting

For experiments presented in Figure 5K, cells developed with cAMP pulses for 4 h were washed with cold DB, resuspended in DB to a density of 2×10^7 cells/mL, and kept on ice before stimulation. Cells were stimulated at room temperature with the addition of cAMP with a final concentration of 1 μM, lysed with 3× sample buffer, and boiled for 5 min.

For λ-phosphatase treatment, WT cells expressing Hbx5^M-GFP were collected before and after cAMP stimulation, lysed at a density of 2×10^7 cells/mL by adding equal volume of 2 × lysis buffer [20 mM sodium phosphate (pH 7.2), 100 mM NaCl, 1% (vol/vol) Nonidet P-40, 100 mM NaF, 50 mM sodium pyrophosphate, 4 mM Na_3VO_4, 2 × complete EDTA-free protease inhibitor cocktail], and incubated on ice for 5 min. Lysates were centrifuged at 22,000 × g for 5 min. 600 μL of supernatant was incubated with 10 μL anti-GFP affinity beads at 4°C for 2 h. Following washes with buffer [10 mM sodium phosphate (pH 7.2), 50 mM NaCl, 0.5% Nonidet P-40, 1× complete EDTA-free protease inhibitor cocktail], the beads were washed with and resuspended in 20 μL phosphatase buffer (NEB). Reaction was initiated by the addition of 0.5 μL λ-protein phosphatase (NEB), allowed to proceed for 20 min at 30°C, and stopped by the addition of 15 μL 3× sample buffer.

For experiments presented in Figure 5M, cells developed in suspension with cAMP pulses for 4 h were collected before or at different time points after the addition of pulses of cAMP, lysed with 3× sample buffer, and boiled for 5 min.

For experiment presented in Figure S7E, growth stage cells were washed once with DB and resuspended in DB at a density of 2×10^7 cells/mL. The cells were incubated in DB for 30 min before stimulating with 1 mM folic acid. Samples were collected at different time points, lysed with 3× sample buffer, and boiled for 5 min.

To resolve the mobility shift of Hbx5^M-GFP, proteins were separated on 8 % Tris·HCl polyacrylamide gels. Anti-Phospho-Threonine/Tyrosine antibody (WB, 1:1000) was purchased from Cell Signaling Technology. Anti-Phospho-p44/42 MAPK antibody (WB, 1:1000) from Cell Signaling Technology was used to detect phosphorylation of the ErkB kinase.

Phalloidin staining

For microscopy imaging, cells were plated in coverslip chamber and allowed to adhere. Cells were fixed for 8 min at room temperature with 2% paraformaldehyde and 0.4% glutaraldehyde in KK2, permeabilized for 8 min with the addition of 0.2% TX-100, quenched in PBS containing 20 mM glycine, and washed with KK2. Cells were then stained with 14 μM Acti-stain 555 phalloidin at room temperature in the dark for 30 min. Extra phalloidin was washed away before imaging. For flow cytometry analysis, cells were resuspended in KK2 at 2×10^6/mL, and then fixed and stained following the aforementioned procedures. Subsequently, cells were washed and resuspended in KK2 prior to analysis. The total fluorescence intensity per cell was determined by a BD Biosciences Influx flow cytometer, and the data were analyzed using FlowJo_v10.8.1.

RT-qPCR

For experiments presented in Figure 7L, *crac*$^-$ cells were starved in DB for 2 h at 2×10^7 cells/mL, and then pulsed with 50 nM cAMP applied at different intervals for 2 h. Total RNA was extracted from cells using Trizol (Ambion) and reverse-transcribed using the PrimeScript RT reagent kit with gDNA Eraser (Takara). Quantitative real-time PCR was performed using SYBR Green PCR Master Mix (TaKaRa) and CFX96 Real-Time System (Bio-Rad). *Ig7* was used as a reference gene. Primers used for RT-qPCR are listed in Table S3. For experiments presented in Figure S4D, total RNA was extracted from cells grown in HL5 medium.

Please cite this article in press as: Hao et al., A transcription factor complex in *Dictyostelium* enables adaptive changes in macropinocytosis during the growth-to-development transition, Developmental Cell (2024), https://doi.org/10.1016/j.devcel.2024.01.012

CellPress

Whole-transcriptome RNA-Seq

RNA samples were collected from growth stage WT, *hbx5*$^{-}$, and *mybG*$^{-}$ cells and sent to Berry Genomics (Beijing, China) for sequencing. Quality control was conducted using fastQC.[51] Trim Galore (https://www.bioinformatics.babraham.ac.uk/projects/trim_galore/) was used to trim adaptors with the default parameters, and retain reads that longer than 100 bases. The clean reads were mapped to the reference genome (GCA_000004695.1) using Bowtie2.[52] Transcript quantification was processed by StringTie.[53] DEseq2[54] was implemented to identify differentially expressed genes using a fold change cutoff of 1.5 against AX2. The false discovery rate (FDR) method was used for correcting multiple comparisons and a FDR cutoff of 0.05 was applied. Hbx5 and MybG co-regulated target candidates were identified among differentially expressed genes based on the co-upregulated or co-downregulated genes using in-house Perl scripts. GO analysis was carried out using the plugin of BiNGO in Cytoscape.[55]

ChIP-seq

Chromatin immunoprecipitation (ChIP) experiment was performed as described previously[42] with minor modifications. WT cells expressing MybG-GFP or GFP were harvested at 5 × 10^7/mL and incubated with 1% paraformaldehyde in KK2 at room temperature to crosslink. After 5 min, glycine was added to terminate the crosslinking reaction. After washing with KK2, cells were resuspended in buffer [40 mM Tris-HCl (pH 7.8), 6 mM $MgCl_2$, 40 mM KCl, 0.1 mM EDTA, 5 mM dithiothreitol, 1.5% Sucrose, 0.4% Nonidet P-40] on ice for 10 min. Samples were centrifuged at 4°C. The pellet was then resuspended in ice-cold lysis buffer [50 mM Tris-HCl (pH 8.0), 150 mM NaCl, 2 mM EDTA, 1% Triton X-100, 0.05% SDS, complete EDTA-free protease inhibitor cocktail]. Chromatin samples were sheared to 100–300 bp fragments using the Bioruptor sonication device (20 cycles of 30 sec ON/30 sec OFF). After a brief centrifugation, the nuclear extracts were incubated on ice for 30 min and centrifuged again at 22,000 × g for 15 min. The supernatants were pre-cleared using protein G Dynabeads (Invitrogen) at 4°C for 1 h. The pre-cleared supernatants were then incubated with 25 μL protein G Dynabeads with (2.4 μg) or without anti-GFP antibodies (abcam) at 4°C overnight. The beads were washed sequentially with lysis buffer, high-salt buffer, LiCl-wash buffer, and TE buffer, and eluted with 100 μL elution buffer twice at 65°C for 15 min. The combined eluates were incubated at 65°C overnight to reverse crosslinking. 240 μL TE buffer, proteinase K (final 500 μg/mL), and RNase (10 μg/mL) were added and the samples were incubated at 37°C for 1-2 h. The ChIP DNA was extracted once with phenol/chloroform, once with chloroform, and then precipitated with ethanol and glycogen. After air-dry, the DNA pellet was resuspended in 30 μl TE buffer. Sequencing was performed by Jiayin Biotechnology (Shanghai, China).

The raw data was checked using Trim Galore to remove remaining adaptors. The clean data were mapped to the reference genome (GCA_000004695.1) using Bowtie2[52] allowing no more than one mismatch, and only the best-mapped site for each read was retained. Samples with a low mapping rate (<50%) were discarded. The binding peaks were called using MACS2[56] with default parameters except the FDR as 0.01. Fold of enrichment was calculated between MybG-GFP and GFP input with 2 as cutoff.

QUANTIFICATION AND STATISTICAL ANALYSIS

Quantification

To quantitate the period of nucleocytoplasmic shuttling of Hbx5 and MybG as presented in Figures 5B, 6B, 6F, S6A, S6B, S6D, and S6G, a user-developed MATLAB script was employed to extract the mean nuclear intensity of GFP and RFP. To this end, the channel of GFP and RFP signals were separated into two different movies. For each frame of movies, the image was converted to a gray one by the MATLAB built-in function rgb2gray. The magnitude of the gray image matrix denotes the intensity of signal. We then extracted the nuclear domain from the gray image. The MATLAB built-in function Im2bw was employed to convert gray images to binary functions. Some morphological operations were implemented in MATLAB and the nuclear domain was labeled. Next, in each nuclear domain, the average intensity of signals was calculated, through which the time sequence of the intensity of GFP and RFP of each nucleus was acquired. At time t, ratio between GFP and RFP was calculated by

$$I_{G/R}(t) = \frac{I_{GFP}(t)}{I_{RFP}(t)},$$

where $I_{GFP}(t)$ and $I_{RFP}(t)$ represent the mean intensity of GFP and RFP of all nuclear domains per frame, respectively.

To quantify the speed of cell movement, videos were analyzed using the mTrackJ plug-in. Cells moved out of the imaging field during the video were excluded from the analysis. The average speed was plotted against time.

The temporal auto-correlation function is formulated by

$$acf(dt) = \frac{1}{N}\sum_{t}\frac{(I(t) - \mu)\cdot(I(t+dt) - \mu)}{\sigma^2},$$

where $I(t)$ denotes either the intensity of nuclear GFP/RFP or the magnitude of cell speed. μ and σ are the average and standard deviation of $I(t)$ over all time sequences. N is the number of time samples and summation is implemented over all time samples.

To quantify migration parameters, including accumulated distance, Euclidean distance, and velocity, cells were tracked using the manual tracking plugin of Fiji ImageJ and analyzed using Ibidi chemotaxis tool software.

Please cite this article in press as: Hao et al., A transcription factor complex in *Dictyostelium* enables adaptive changes in macropinocytosis during the growth-to-development transition, Developmental Cell (2024), https://doi.org/10.1016/j.devcel.2024.01.012

Statistical analysis

Statistical analysis was performed using GraphPad Prism 9.0. Statistical significance was determined by one-way ANOVA with Dunnett post-test or two-tailed unpaired t test with Welch's correction. In all figures, *** indicates $p < 0.001$, ** $p < 0.01$, * $p < 0.05$, and ns not significant. The statistical details for every experiment (number of replicates, nature of statistical tests, and meaning of symbols used to show significance) are mentioned in the figure legends.